Influence of mixing on CFC uptake and CFC ages in the North Pacific thermocline

Sabine Mecking
Woods Hole Oceanographic Institution, Woods Hole, Massachusetts, USA

Mark J. Warner, Catherine E. Greene, and Susan L. Hautala
School of Oceanography, University of Washington, Seattle, Washington, USA

Rolf E. Sonnerup
Joint Institute for the Study of the Atmosphere and Ocean, University of Washington, Seattle, Washington, USA

Received 31 May 2003; revised 20 February 2004; accepted 13 May 2004; published 17 July 2004.

[1] A diagnostic, isopycnal advection-diffusion model based on a climatological, geostrophic flow field is used to study the uptake of chlorofluorocarbons (CFCs) into the portion of the thermocline that outcrops in the open North Pacific ($\sigma_\theta \leq 26.6$ kg m^{-3}). In addition to advection, isopycnal diffusion is required to match the CFC data collected during the World Ocean Circulation Experiment (WOCE) in the early 1990s. Using reduced outcrop saturations of 80–95% for isopycnals outcropping in the northwestern North Pacific ($\sigma_\theta \geq 25.4$ kg m^{-3}), together with an isopcynal interior diffusivity of 2000 m^2 s^{-1} and enhanced diffusion (5000 m^2 s^{-1}) in the Kuroshio Extension region, further improves the model-data agreement. Along-isopycnal diffusion is particularly important for isopycnals with shadow zones/pool regions in the western subtropical North Pacific that are isolated from direct advective ventilation. The isopycnal mixing causes an estimated increase in CFC-12 inventories on these isopycnals, compared to advection only, ranging from 10–20% ($\sigma_\theta = 25.6$ kg m^{-3}) to 50–130% ($\sigma_\theta = 26.6$ kg m^{-3}) over the subtropics in 1993. This contribution has important consequences for subduction rate estimates derived from CFC inventories and for the location of the subsurface CFC maxima. When tracer ages are derived from the modeled CFC distributions, time-evolving mixing biases become apparent that reflect the nonlinearities in the atmospheric CFC time histories. Comparison with model-calculated ideal ages suggests that during the time of WOCE ($\sim$1993), ventilation ages based on CFC-12 were biased young by as much as 16–24 years for pCFC-12 ages of 25 years, underestimating ideal ages by as much as 40–50%. *INDEX TERMS:* 4808 Oceanography: Biological and Chemical: Chemical tracers; 4568 Oceanography: Physical: Turbulence, diffusion, and mixing processes; 4532 Oceanography: Physical: General circulation; 4255 Oceanography: General: Numerical modeling; 9355 Information Related to Geographic Region: Pacific Ocean; *KEYWORDS:* tracers, mixing, thermocline

Citation: Mecking, S., M. J. Warner, C. E. Greene, S. L. Hautala, and R. E. Sonnerup (2004), Influence of mixing on CFC uptake and CFC ages in the North Pacific thermocline, *J. Geophys. Res.*, *109*, C07014, doi:10.1029/2003JC001988.

1. Introduction

[2] Chlorofluorocarbons (CFCs) have proven to be useful oceanographic tracers that can be applied to a variety of problems. CFC concentration fields can be helpful in determining ventilation pathways and in identifying water masses [e.g., *Warner and Weiss*, 1992; *Fine*, 1993; *Fine et al.*, 1994; *Warner et al.*, 1996; *Smethie et al.*, 2000], and water mass renewal rates can be estimated from the integrated CFC content (CFC inventories) [*Orsi et al.*, 1999; *Smethie and Fine*, 2001]. CFC ages derived from the concentration fields provide important information on ventilation timescales [*Doney and Bullister*, 1992; *Warner et al.*, 1996], which have been used to estimate oxygen utilization [*Warner et al.*, 1996; *Sonnerup et al.*, 1999; *Abell et al.*, 2000; *Min et al.*, 2000; *Feely et al.*, 2004] and organic matter remineralization rates [*Abell et al.*, 2000] and anthropogenic CO_2 inventories [*Sabine et al.*, 1999; *Watanabe et al.*, 2000; *Sabine et al.*, 2002]. Age comparisons between repeated hydrographic sections can also help detect changes in ocean ventilation [*Doney et al.*, 1998; *Mecking*, 2001; *Watanabe et al.*, 2001; S. Mecking et al., Age and AOU increases at the North Pacific subtropical/subpolar gyre boundary, submitted to *Deep-Sea Research*, 2004, hereinafter referred to as Mecking et al., submitted

0148-0227/04/2003JC001988$09.00

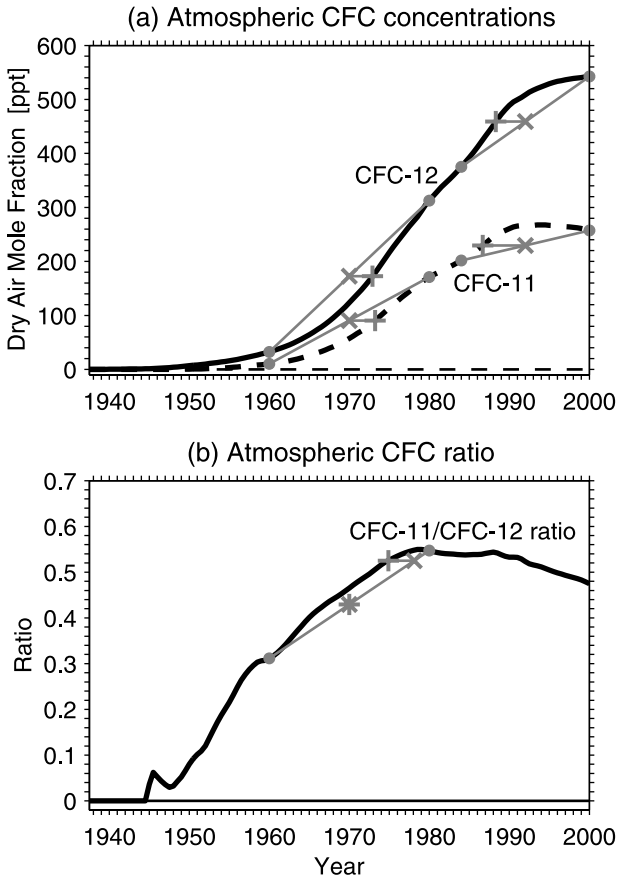

Figure 1. Atmospheric time history of (a) CFC-11 and CFC-12 concentrations and (b) the ratio of CFC-11 over CFC-12. Data are from *Walker et al.* [2000], augmented by an air measurement for 2000 from our own archives. Shaded lines and symbols give examples of the nonlinear mixing that occurs between two end-members (shaded dots). In Figure 1a, crosses mark the average year and concentration of the end-members, and plusses mark the projection of the average concentrations onto the atmospheric curves. In Figure 1b the asterisk marks the average ratio and year of the end-members, the cross marks the ratio and year that result from mixing CFC-11 and CFC-12 independently (see Appendix A), and the plus marks the projection of the mixed ratio onto the atmospheric curve.

manuscript, 2004]. For all of these applications, it is important to understand the effects that advection and diffusion have in generating the observed tracer distributions. Of particular interest are the biases in the CFC-derived ventilation ages that can occur in the presence of ocean mixing. One method of estimating the ventilation ages is to project the apparent CFC partial pressure of a water sample, which is defined as

$$\mathrm{pCFC} = \frac{C}{f_{\mathrm{sat}} F_{\mathrm{sol}}(\theta, S)} \tag{1}$$

[*Doney and Bullister*, 1992; *Warner et al.*, 1996], onto the atmospheric concentration history (Figure 1a) and to subtract the resulting year from the time of measurement. Here C is the measured CFC-12 or CFC-11 concentration, F_{sol} is the temperature-dependent and salinity-dependent solubility function [*Warner and Weiss*, 1985], and f_{sat} is the gas saturation state when the water left the surface, usually assumed to be 100% (i.e., $f_{\mathrm{sat}} = 1$) unless it is known that the water was not in equilibrium with the atmosphere. The main reason for biases in these ages, referred to as pCFC-12 and pCFC-11 ages, is that the atmospheric CFC time histories are nonlinear [*Doney et al.*, 1997]. Depending on the curvature of the time histories, the nonlinearities can cause the year that corresponds to the projection of the average pCFC of two end-members onto the time history to be either younger or older than the true average year of the end-members (Figure 1a). Accordingly, the pCFC ages can be younger or older than the true average age of the end-members as well. If the ratio of pCFC-11/pCFC-12 [*Weiss et al.*, 1985; *Warner et al.*, 1996] is used to estimate ventilation ages (referred to as pCFC ratio ages) instead, mixing biases can occur not only due to nonlinearities in the atmospheric CFC-11/CFC-12 history but also because the CFC-11/CFC-12 ratio of the mixture of two end-members is biased toward the end-member with the higher CFC-12 concentrations (Figure 1b, see Appendix A), which is generally the younger component.

[3] In this paper we attempt to quantify the effects of advection and diffusion in the North Pacific thermocline with a diagnostic thermocline model that is based on geostrophic velocities calculated directly from climatological data. The model is used to simulate CFC distributions and to calculate ideal tracer ages for comparison. Since thermocline ventilation occurs predominantly along isopycnals [*Iselin*, 1939; *Jenkins*, 1980; *Luyten et al.*, 1983; *Sarmiento*, 1983; *Robbins et al.*, 2000], model integrations are performed on isopycnal surfaces that outcrop in the North Pacific. Isopycnal diffusion is used to tune the model to CFC observations made as part of the World Ocean Circulation Experiment (WOCE) Hydrographic Program in the North Pacific in the early 1990s. The influence of vertical diffusion, however, is also considered. Our diagnostic model is an extension of previous thermocline models using one-dimensional pipe flows [*Warner and Weiss*, 1992; *Sonnerup et al.*, 1999; *Sonnerup*, 2001] or two-dimensional, idealized flow fields based on a Stommel gyre [*Musgrave*, 1985, 1990; *Thiele and Sarmiento*, 1990; *Doney et al.*, 1997; *Robbins et al.*, 2000] to investigate the behavior of transient tracers for varying strengths of circulation and mixing. The advantage of our diagnostic model is that it uses observation-based velocities and realistic outcrop and basin geometries so that we can compare and combine the modeled tracer fields directly with observations. For instance, model estimates of CFC age biases may be applied as corrections to data-derived CFC ages, and the best-fit mixing scheme provides an estimate of isopycnal diffusion rates.

[4] The remainder of the paper is structured as follows: The formulation of the model and its sensitivity toward diffusion and outcrop boundary conditions are described in sections 2 and 3, respectively. Model results are described in section 4, with focus on the influence of mixing on the subsurface CFC-12 maximum, the CFC-12 inventories, and the CFC ages in sections 4.1, 4.2, and 4.3,

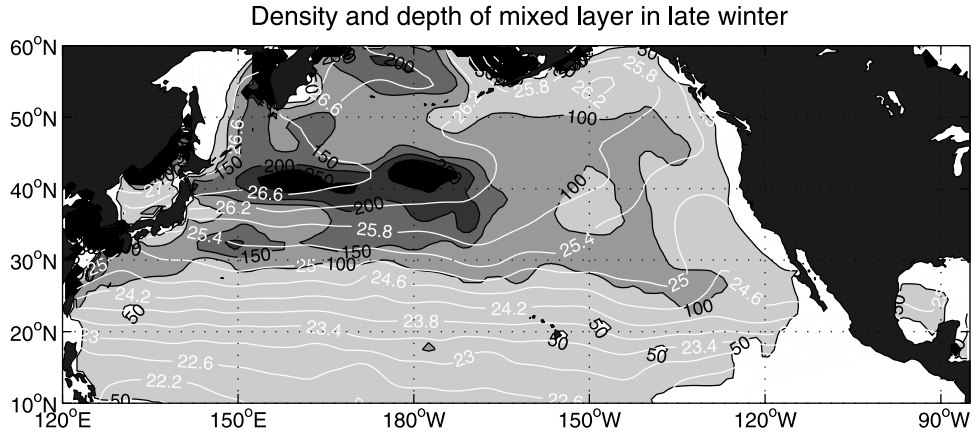

Figure 2. Density anomaly at the base of the March mixed layer (white contours) and maximum mixed layer depth (occurring usually in late winter; color shading and black contours) based on the Levitus 1994 climatology [*Levitus et al.*, 1994; *Levitus and Boyer*, 1994]. The base of the mixed layer is defined by a density increase of 0.125 kg m^{-3} from the surface density.

respectively. Discussion and summary are presented in section 5.

2. Model Description

[5] Following the idea that water properties in the thermocline are determined by the mixed layer properties in late winter [*Iselin*, 1939; *Stommel*, 1979; *Cushman-Roisin*, 1987], the northern boundary of the model domain is defined as the March mixed layer outcrop location of each modeled isopycnal (Figure 2). Salinity and temperature data from *Levitus et al.* [1994] and *Levitus and Boyer* [1994], respectively (hereinafter referred to as the Levitus 1994 climatology), are used to determine these locations, assuming that the base of the mixed layer is denser than the surface by 0.125 kg m^{-3} [*Levitus*, 1982]. The southern boundary of the model is set at 10°N, the approximate southern extent of the subtropical gyre, for all isopycnals. Model integrations are performed for σ_θ = 23.0–26.6 kg m^{-3} in intervals of 0.2 kg m^{-3}, thus including all isopycnals that outcrop in the North Pacific to the north of ~15°N. The model resolution is the 1° × 1° grid of the Levitus 1994 climatology.

2.1. Velocity Field

[6] Annual mean geostrophic velocities calculated from the Levitus 1994 climatology are used to simulate the advective transport of water and tracers from the outcrops into the interior of the subtropical gyre and, for isopycnals that outcrop far enough to the north, into the subpolar gyre interior. The velocities are determined from the horizontal gradients in acceleration potential [*Montgomery*, 1937; *Reid*, 1965] using a reference level of 1500 m.

[7] On the deeper (and denser) isopycnals, the acceleration potential contours, as shown for σ_θ = 26.0 kg m^{-3} (Figure 3), show a region of closed streamlines within the western part of the subtropical gyre that is not ventilated through advection from the outcrop. Isolated pool regions like this [*Luyten et al.*, 1983], which we call western shadow zones (WSZs), exist for $\sigma_\theta \geq$ 25.4 kg m^{-3} because these isopycnals outcrop in the northern half of the subtropical gyre. The extent of each isopycnal's WSZ can be described by determining the densest isopycnal for each grid point (on the 1° × 1° grid) for which an intersection between acceleration potential and outcrop is found (Figure 4). A grid point within the subtropical gyre belongs to the WSZ of an isopycnal if the density of the isopycnal is greater than the bottom of the advectively ventilated thermocline determined by this method. The size of the WSZ increases with density: It is confined to a small area in the western Pacific between ~130°E and ~150°E for σ_θ = 25.4 kg m^{-3} but covers most of the subtropical gyre for σ_θ = 26.6 kg m^{-3}, the densest isopycnal in the model. Our calculations indicate that in the western subtropical gyre the bottom of the advectively ventilated thermocline is at or below the Subtropical Mode Water (STMW), the density of which increases going eastward from σ_θ = 25.2 kg m^{-3} at ~140°E to σ_θ = 25.4 kg m^{-3} at ~160°E [*Bingham*, 1992]. STMW being part of the advectively ventilated thermocline agrees with the suggestion by *Bingham* [1992] that "differential spreading" of STMW from the outcrops into the ocean interior occurs along streamlines.

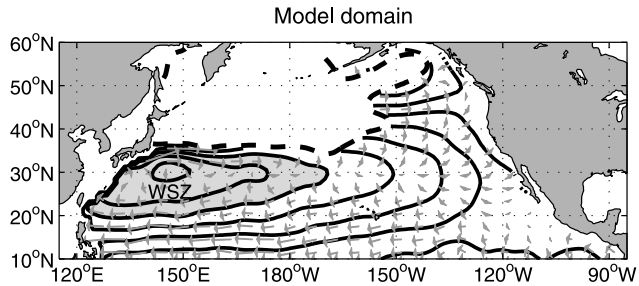

Figure 3. Domain of the advection-diffusion model illustrated for σ_θ = 26.0 kg m^{-3}. Solid lines mark acceleration potential contours derived from the Levitus 1994 climatology and including a constant value correction at the western boundary (see text). Vectors are the corresponding velocity vectors. The dashed line marks the March outcrop locations of the isopycnal. The shaded area marks the western shadow zone (WSZ) of this isopycnal.

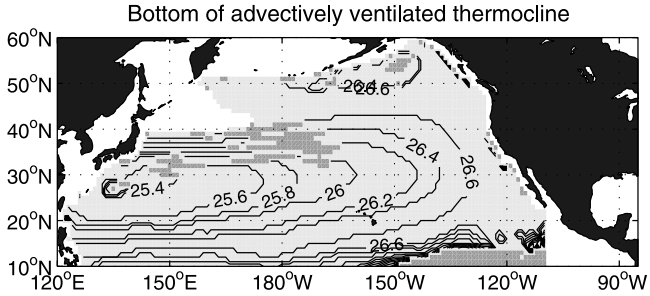

Figure 4. Potential density anomaly at the bottom of advectively ventilated thermocline determined by tracing acceleration potential contours for σ_θ = 23.0–26.6 kg m^{-3} (in 0.2 kg m^{-3} increments) back to the March outcrops (see text). Light shading marks the area examined, and intermediate shading marks areas where the bottom of the advectively ventilated thermocline could not be determined, probably due to the grid resolution.

[8] Figure 4 is not an exact description of the bottom of the advectively ventilated thermocline, however, because small errors in the outcrop location of isopycnals, particularly in the Kuroshio Extension region of Japan, where streamlines are close together (Figure 3), could alter size and density of the WSZs. Uncertainties in the climatological outcrop locations arise due to the bulk formula estimate of the density at the base of the mixed layer (see above) and possible interannual variations. Although the choice of reference levels within the range commonly used in studies of the upper North Pacific (1000–2000 m) [*Reid*, 1961; *Yuan and Talley*, 1992; *Huang and Qiu*, 1994; *Qu et al.*, 1998] has little impact on the resulting velocity field, the choice of climatology may affect the extent of the WSZs too [*Mecking*, 2001]. The Levitus 1994 climatology is chosen here over the more recent, isopycnally averaged Hydrobase climatology [*Grey et al.*, 1999; *MacDonald et al.*, 2001] because the latter includes data gaps that lead to unrealistic circulation features in the eastern North Pacific [*Mecking*, 2001], even though a sophisticated smoothing algorithm was employed [*Grey et al.*, 1999].

2.2. Boundary Conditions

[9] CFC concentrations at the outcrops (C_{outcrop}) are calculated from a reversed form of equation (1):

$$C_{\text{outcrop}}(T,S,t) = f_{\text{sat}} \cdot F_{\text{sol}}(T,S) \cdot X_{\text{atmos}}(t), \qquad (2)$$

where X_{atmos} is the time-dependent atmospheric concentration (Figure 1a), F_{sol} are the CFC solubility functions [*Warner and Weiss*, 1985] based on March mixed layer temperature and salinity from the Levitus 1994 climatology, and f_{sat} is the factor describing the gas saturation state at the outcrop (f_{sat} = 1 for 100% saturation). For the ideal age tracer the age at the outcrop is reset to zero at every time step.

[10] At the 10°N open boundary a constant age condition is applied for both CFCs and the ideal age tracer using pCFC-12 ages based on the early 1990s U.S. WOCE sections (P10, P13, P14, P16, P17, P18, P19) [*World Ocean Circulation Experiment Data Products Committee* (*WOCEDPC*), 2002]. The ages were determined by interpolating the pCFC-12 ages to density levels, mapping them on a 1° × 1° grid for each isopycnal, and then subsampling the grid at 10°N (Figure 5). For the ideal age tracer the southern boundary condition is directly specified by this age. For CFCs the boundary condition ($C_{10°\text{N}}$) evolves over time and is described by

$$C_{10°\text{N}} = F_{\text{sol}}(\theta,S) \cdot X_{\text{atmos}}(t-\tau), \qquad (3)$$

where F_{sol} is the solubility function based on annual temperature and salinity data from the Levitus 1994 climatology and τ is the age of the water estimated by the pCFC-12 ages. As we argue in this paper, pCFC-12 ages are substantially biased through mixing (see section 4.3), and hence the WOCE pCFC-12 ages at 10°N do not present the true age of the water accurately.

[11] However, since water is carried northward across 10°N only in the easternmost portion of this zonal section (Figure 3), the southern boundary condition is much less important than the outcrop boundary condition. Comparison of model experiments, including diffusion with different boundary conditions at 10°N, shows that for CFCs the southern boundary influences model results as far north as ~18°N [*Mecking*, 2001]. The different specifications of ages along 10°N, however, change the ideal ages more than the CFCs such that ideal ages on $\sigma_\theta \geq$ 26.2 kg m^{-3} are affected throughout the subtropical gyre through diffusion from the southern boundary. On the model's lighter isopycnals ($\sigma_\theta \leq$ 26.0 kg m^{-3}), where the advective fluxes within the subtropical gyre are stronger, the effects of the southern boundary on ideal ages extend to only ~18°N as well. The sensitivity of the ideal ages to the southern boundary condition for $\sigma_\theta \geq$ 26.2 kg m^{-3} is examined by multiplying the WOCE pCFC-12 ages at 10°N (Figure 5) by factors of 1.5 and 2, which accounts for possible biases in the age boundary condition (see section 4.3).

[12] At the eastern and western boundaries, corrections to the velocity fields are applied to avoid advective fluxes into

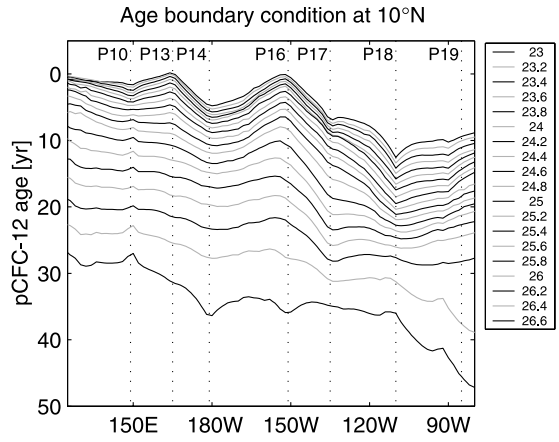

Figure 5. Age boundary condition at 10°N based on isopycnal maps of pCFC-12 ages derived from the early 1990s meridional U.S. WOCE sections (see text). Ages increase with density, and age graphs are alternately drawn as dark and shaded lines for increasing density anomaly (as described in legend). The dotted lines mark the longitudes of the WOCE lines at 10°N.

and out of the continents that are caused by the limited resolution and by the smoothing of the Levitus 1994 climatology. The circulation at the western boundary is closed by setting the acceleration potential along the boundary to a constant value before calculating the geostrophic velocities (see Figure 3, where this correction is already included). The constant boundary value is determined by the acceleration potential at the bifurcation point of the North Equatorial Current (NEC) following the method of *Qu et al.* [1998]. Consistent with a northward shift of the subtropical gyre with depth [*Reid*, 1997], the latitude of this bifurcation point increases with density from ~14°N at σ_θ = 23.0 kg m^{-3} to ~17.5°N at σ_θ = 26.6 kg m^{-3} [*Greene*, 2000; *Mecking*, 2001]. Along North and Central America the velocities normal to the coastline, which are usually small, are set to zero.

2.3. Model Equations

[13] Assuming that isopycnal diffusion is isotropic ($\kappa_x = \kappa_y \equiv \kappa_h$), the two-dimensional advection-diffusion equation for a conservative tracer on a sphere in local *x*-*y* coordinates is

$$\frac{\partial C}{\partial t} = -\nabla \cdot (C\mathbf{u}) + C\nabla \cdot \mathbf{u} + \frac{1}{h}\nabla \cdot (h\kappa_h \nabla C) - \kappa_h \frac{\partial C}{\partial y}\frac{\tan\theta}{R_E}, \quad (4)$$

where C is the tracer concentration, $\mathbf{u}$ is the two-dimensional, horizontal velocity vector, h is the thickness of the isopycnal layer, θ is latitude, and R_E is the radius of the Earth. For the model the thickness of each isopycnal layer is calculated from the depth difference between σ_θ + 0.1 kg m^{-3} and σ_θ − 0.1 kg m^{-3} in the annual Levitus 1994 climatology. Given these layer thicknesses, the model is not fully mass conserving because the divergence of the geostrophic velocities is not always compensated by the gradients in layer thickness. Diapycnal mass fluxes, barotropic velocity components, and ageostrophic velocities, which are neglected in the model, must be responsible for the discrepancies. The contribution of the layer thickness gradient to the diffusion terms is of minor importance.

[14] Assuming a time-dependent, conservative tracer with linearly increasing source function and constant solubility, equation (4) can be converted to a conservation equation for ideal tracer age (A_{ideal}) [*Thiele and Sarmiento*, 1990; *Doney et al.*, 1997; *Mecking*, 2001], which differs in its structure from equation (4) only through the additional term of +1:

$$\frac{\partial A_{\text{ideal}}}{\partial t} = -\nabla \cdot (A_{\text{ideal}}\mathbf{u}) + A_{\text{ideal}}\nabla \cdot \mathbf{u} + \frac{1}{h}\nabla \cdot (h\kappa_h \nabla A_{\text{ideal}}) - \kappa_h \frac{A_{\text{ideal}}}{\partial y}\frac{\tan\theta}{R_E} + 1. \quad (5)$$

Equations (4) and (5) are integrated on a C grid using an advection scheme with small implicit diffusion for the balance between the time derivative and the first advective term [*Smolarkiewicz*, 1984]. The other terms in the equations are solved using centered differencing. The CFCs are time integrated starting in the 1930s, when CFCs were first introduced into the atmosphere, until 2000, and the ideal age tracer is run to steady state.

[15] While model integrations are performed for each isopycnal separately, vertical sections and profiles can be created by combining the model results into a three-dimensional field. In an extended version of the model the layers are coupled during the integrations to investigate the effects of diapycnal diffusion. In this case, all layers are stepped forward simultaneously, and an additional diapycnal diffusion term that connects the layers is added to the advection-diffusion equations. To take care of the now necessary bottom boundary condition, a quasi-infinite bottom domain, which is ventilated only through diffusion from above, is added to the model domain. However, the standard model case is without the coupling of the layers and without the bottom domain.

3. Role of Diffusion and Outcrop Boundary Conditions

[16] The model's performance is evaluated by comparison to CFC-12 concentration data from the early 1990s U.S. WOCE sections [*WOCEDPC*, 2002]. The data are first corrected to January 1993, the approximate midpoint of the cruises, using an age correction technique [*Warner et al.*, 1996] based on the pCFC-12 ages. The age-corrected data are then interpolated to isopycnal surfaces and objectively mapped onto a horizontal grid. Because of the nonlinear mixing biases associated with the pCFC-12 ages (see sections 2.2 and 4.3), the age correction is not accurate. However, in the interest of having a synoptic data set, we use this correction, which changes concentrations on ispycnal surfaces by averages of 2% (σ_θ = 23.0 kg m^{-3}) to 15% (σ_θ = 26.6 kg m^{-3}) and mean isopycnal concentrations by <3% for all isopycnals. Since CFC-11 and CFC-12 usually show very similar behavior in ocean models, only one of these tracers is necessary to examine a model's performance [*Dutay et al.*, 2002]. CFC-12 is chosen here because its increasing atmospheric source function (Figure 1a) allows unique determination of pCFC-12 ages through the 1990s. In sections 3.1–3.4 we focus on σ_θ = 26.0 kg m^{-3} to illustrate the model's behavior.

3.1. Advection Only

[17] In CFC-12 model integrations based on advection only, the WSZs remain largely unventilated, as shown for σ_θ = 26.0 kg m^{-3} (Figure 6a), because the closed streamlines of the WSZs do not intercept the outcrops. Tracer concentrations in the WSZs are small but are greater than zero due to a small amount of numerical diffusion and, more importantly, due to implicit, grid-size-induced mixing at the western boundary, where streamlines within the western boundary current (WBC) are very close together (Figure 3). Outside the WSZs, tracer concentrations closely follow the curving path of the streamlines. This is in contrast to the WOCE observations, which show high concentrations of CFC-12 in the WSZs and mostly zonal isopleths (Figure 6d). Hence ventilation processes other than advection must be effective.

3.2. Diapycnal Diffusion

[18] First-order scaling arguments suggest that isopycnal advection and diffusion occur on faster timescales than diapycnal diffusion in the thermocline. This scaling, however, does not account for complex, three-dimensional circulation patterns (e.g., the vertical shear in the advective

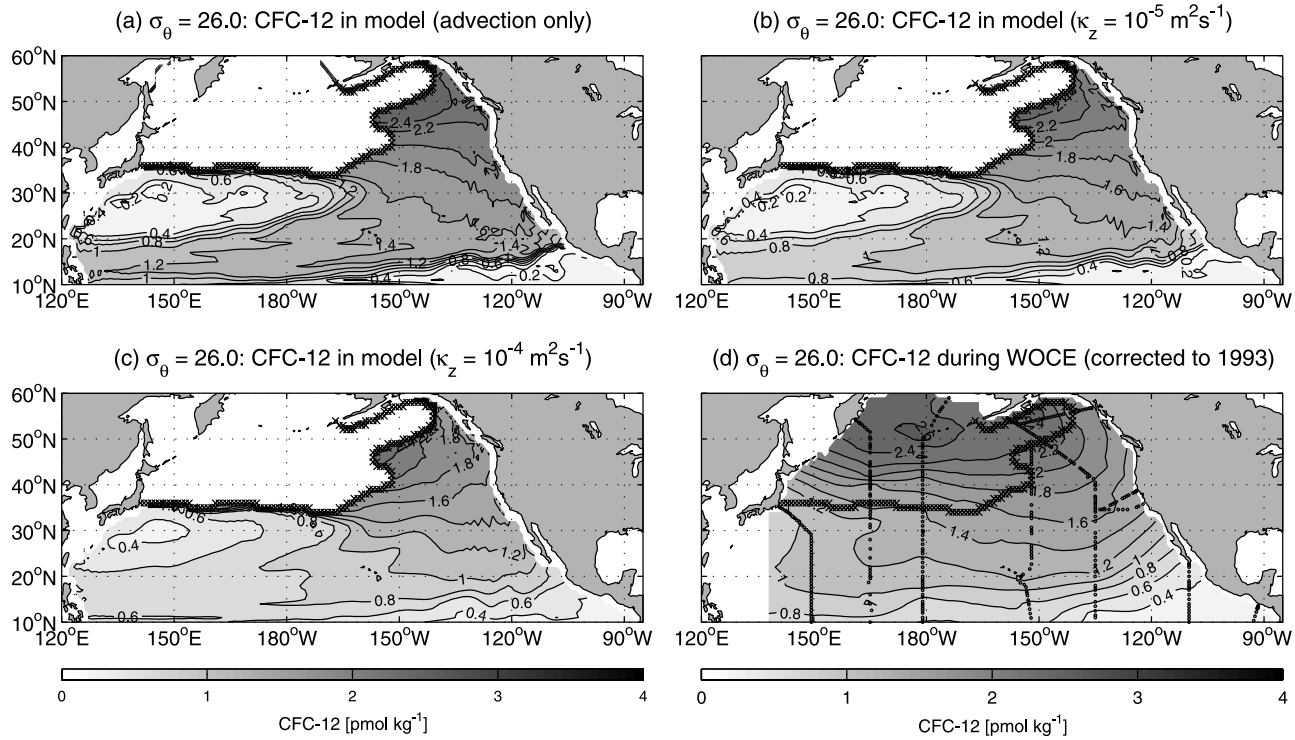

Figure 6. CFC-12 concentrations on σ_θ = 26.0 kg m^{-3}: model results in 1993 (a) for advection only (κ_z = 0 m^2 s^{-1}), (b) with $\kappa_z = 10^{-5}$ m^2 s^{-1}, and (c) with $\kappa_z = 10^{-4}$ m^2 s^{-1}. (d) Data from the early 1990s U.S. WOCE sections corrected to 1993 and mapped onto the isopycnal. Crosses mark March outcrop locations of isopycnal. Dots in Figure 6d indicate locations of data used. All model runs in Figures 6a–6c are without isopycnal diffusion (κ_h = 0 m^2 s^{-1}).

flow) which could enhance the effects of diapycnal diffusion [*Robbins*, 1997]. However, in model runs including diapycnal diffusion, diffusivities on the order of 10^{-5} m^2 s^{-1} (Figure 6b) do not, indeed, significantly alter the tracer distributions on σ_θ = 26.0 kg m^{-3} based on advection only (Figure 6a). Even a diapycnal diffusivity as high as 10^{-4} m^2 s^{-1}, an order of magnitude larger than thermocline values determined from tracer release studies [*Ledwell et al.*, 1993, 1998], is not sufficient to ventilate the WSZs (Figure 6c). When combined with isopycnal diffusion, the effects of diapycnal diffusion also remain small. For instance, adding diapycnal diffusion to model runs with isopycnal advection and diffusion changes the isopycnal CFC-12 inventories (see section 4.2) on the order of 5% or less for $\kappa_z = 10^{-5}$ m^2 s^{-1} and on the order of 10% or less for $\kappa_z = 10^{-4}$ m^2 s^{-1}. Thus diapycnal diffusion is omitted from further model runs to save computational costs, and adjustments to the isopycnal diffusion and also to the saturation factors at the outcrop boundary are used to tune the model.

3.3. Isopycnal Diffusion

[19] Adding isopycnal diffusion using an isotropic diffusivity of 1000 m^2 s^{-1} carries more tracer into the WSZ on σ_θ = 26.0 kg m^{-3} (Figure 7a) and brings the model output more in line with the observations (Figure 6d). However, a tongue of higher concentration water, which wraps around the WSZ, remains more pronounced than in the data. Increasing κ_h to 2000 m^2 s^{-1} further ventilates the WSZ, but the tongue of high CFC-12, although lessened, is still too strong (not shown). Hence in order to match the concentrations in the WSZ better with the observations, while keeping the diffusion in most parts of the subtropical gyre close to isopycnal thermocline diffusivities of 1500–2000 m^2 s^{-1} estimated by other investigators [*Armi and Stommel*, 1983; *Jenkins*, 1991; *Qiu*, 1995], a spatially varying diffusion field with κ_h = 5000 m^2 s^{-1} in the Kuroshio Extension region and κ_h = 2000 m^2 s^{-1} elsewhere (referred to as diffusion case K2000/5000; see overlying contour lines in Figure 7b) is used. High kinetic energy in the region where the Kuroshio splits off the coast of Japan and forms the Kuroshio Extension [*Wyrtki et al.*, 1976; *Stammer*, 1997] supports this choice of diffusion field. The shape of the CFC-12 isopleths now (Figure 7b) matches the observations (Figure 6d) very closely, suggesting that enhanced diffusion due to eddy formation within the Kuroshio/Kuroshio Extension may play an important role in ventilating the WSZs.

[20] Since the location of the isopycnal outcrops may not be exact (see section 2.1), it is also possible that the high CFC-12 concentrations observed in the WSZs imply that the outcrops are somewhat too far north and that a small southward shift of the outcrops in the Kuroshio Extension region could result in increased ventilation of the WSZs. However, we did not pursue the possibility of altering the outcrop locations but focused on adjusting the outcrop saturations to further improve the match between the data and the model.

3.4. Outcrop Saturation

[21] A systematic mismatch between model and data remains on the denser isopycnals for diffusion case

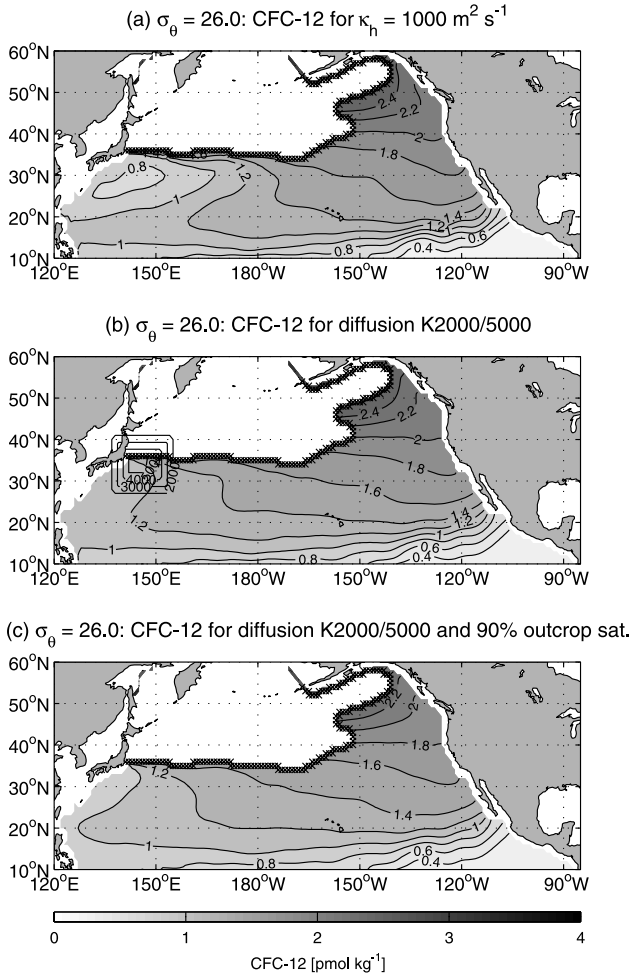

Figure 7. CFC-12 concentrations on σ_θ = 26.0 kg m^{-3}: model results in 1993 with (a) κ_h = 1000 m^2 s^{-1}, (b) κ_h = 5000 m^2 s^{-1} in Kuroshio Extension region and 2000 m^2 s^{-1} elsewhere (diffusion case K2000/5000; contours for the diffusivities are overlaid to mark the patch of higher diffusion to the southeast of Japan), and (c) 90% saturation at the outcrop boundary (also using diffusion case K2000/5000). Crosses mark March outcrop locations of isopycnal. Model runs here and in all following figures are without vertical diffusion (κ_z = 0 m^2 s^{-1}).

K2000/5000. On σ_θ = 26.0 kg m^{-3} the modeled CFC-12 concentrations (Figure 7b) are higher than the observations (Figure 6d) throughout most of the isopycnal, with a root-mean-square (rms) difference of 0.27 pmol kg^{-1} to the north of 18°N (away from the southern boundary, where, through the age boundary condition, data and model are forced to be approximately the same). This discrepancy occurs because the outcrop values in the model assume 100% saturation, whereas the observations indicate that the CFC-12 concentrations along the late winter outcrop boundary are not saturated (see bold crosses in Figures 6d and 7b). Reducing the outcrop saturation for σ_θ = 26.0 kg m^{-3} to 90% in the model (f_{sat} in equation (2) = 0.90) improves the model-data agreement at the outcrop and in the isopycnal interior (Figure 7c), although the modeled tracer concentrations are still too high near the coast of North America, likely because the eastern boundary currents are poorly resolved in the model. The rms difference between data and model is now reduced to 0.15 pmol kg^{-1}.

[22] Assuming undersaturation along the isopycnal outcrop is reasonable because there is a large seasonal cycle in mixed layer depth in the northwestern Pacific, with winter mixed layer depths extending to >150–250 m in the region where $\sigma_\theta \geq$ 25.4 kg m^{-3} outcrop (Figure 2). *Haine and Richards* [1995] showed with a mixed layer model that a seasonal cycle of this size can lead to CFC-12 saturations as low as 85% at the time of deepest mixing (late winter). While the model by *Haine and Richards* [1995] was tuned to the North Atlantic, we estimate, using month-to-month simulations of gas equilibration in the mixed layer based on the Levitus 1994 temperature and salinity climatologies and NCEP wind data (see http://www.cdc.noaa.gov/cdc/data.ncep.reanalysis.derived.html), that the lowest CFC-12 saturations in the North Pacific (in the early 1990s) are also on the order of 85%.

[23] Using the same isopycnal diffusion field (K2000/5000) for the other model isopycnals and varying outcrop saturations of 80–100% (in 5% increments), the following CFC-12 saturations are found to give the best match between the model and the data fields: 100% for $\sigma_\theta \leq$ 25.2 kg m^{-3}, 95% for σ_θ = 25.4–25.8 kg m^{-3}, 90% for σ_θ = 26.0–26.2 kg m^{-3}, 85% for σ_θ = 26.4 kg m^{-3}, and 80% for σ_θ = 26.6 kg m^{-3}. The remaining rms differences amount to ~0.15 pmol kg^{-1} for $\sigma_\theta \geq$ 25.0 kg m^{-3} and less than that for shallower isopycnals. The undersaturations occurring for $\sigma_\theta \geq$ 25.4 kg m^{-3} are in agreement with those isopycnals outcropping where winter mixed layers are deep. The best-fit outcrop saturation for σ_θ = 26.6 kg m^{-3}, being less than the minimum value of 85% saturation based on the mixed layer models described in the paragraph above, may reflect interannual variations in winter mixed layer densities that may have resulted in a temporary or permanent cessation of the outcropping of σ_θ = 26.6 kg m^{-3} [*Emerson et al.*, 2004; Mecking et al., submitted manuscript, 2004].

[24] In addition to σ_θ = 26.0 kg m^{-3}, differences between model and data are illustrated for σ_θ = 25.0 kg m^{-3} (Figures 8a and 8b), where a tongue of high CFC-12 in the eastern part of the subtropical gyre is expressed too strongly in the model, and for σ_θ = 26.4 kg m^{-3} (Figures 8c and 8d), where modeled CFC-12 concentrations are too high in the western subpolar gyre and too low in the eastern subpolar gyre. Some of the differences are likely due to spatial and temporal variations in the CFC outcrop saturations that exist in the real world. However, to keep the model simple, the best overall saturation estimates are used at every point along an isopycnal outcrop.

4. Model Results and Discussion

[25] The tuned model setup (diffusion case K2000/5000 and outcrop saturations as in section 3.4) is used to examine the effects of isopycnal mixing in the North Pacific thermocline on the evolution of the subsurface CFC maxima, on CFC inventories, which can be used to estimate water mass formation rates, and on the time-dependent bias of CFC ages. The focus is again on CFC-12 rather than CFC-11 because of its steadily increasing atmospheric time history. However, when discussing CFC ages, results for pCFC-11

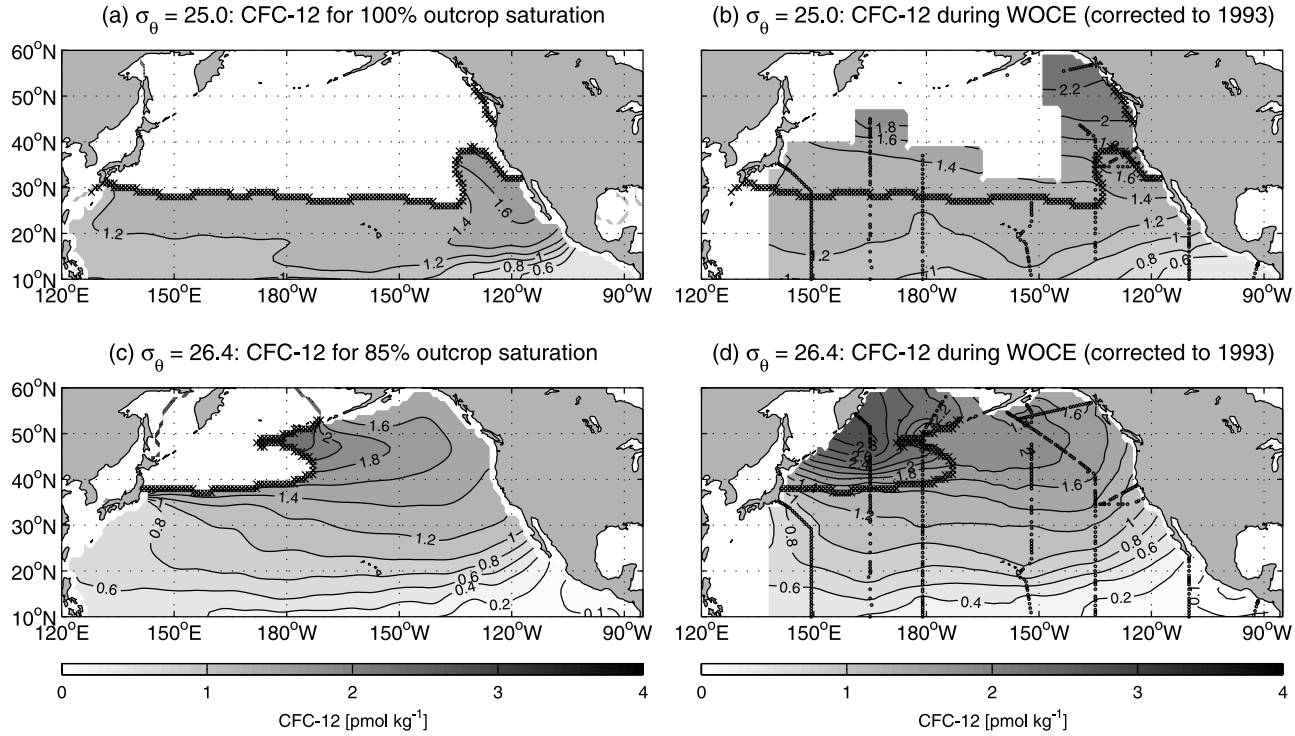

Figure 8. CFC-12 concentrations on σ_θ = 25.0 kg m^{-3} and σ_θ = 26.4 kg m^{-3}: (a, c) model results in 1993 assuming 100% saturation and 85% saturation at the outcrop boundary (diffusion case K2000/5000), respectively, and (b, d) data from the early 1990s U.S. WOCE sections corrected to 1993 and mapped onto the isopycnals, respectively. Crosses mark March outcrop locations of isopycnal. Dots in Figures 8b and 8d indicate locations of data used.

ages and pCFC-11/pCFC-12 ratio ages are also included because these have been widely used in the past.

4.1. CFC-12 Maximum

[26] Subsurface CFC maxima are observed throughout the North Pacific thermocline [*Warner et al.*, 1996; *Mecking and Warner*, 2001]. Examination of the CFC-12 maximum in the model provides another test of the model's performance as well as information about the evolution of the CFC maxima with time.

[27] Within the subtropical gyre the model-predicted spatial structure and the density of the maximum agrees well with the early 1990s U.S. WOCE cruises (see σ_θ = 25.4 kg m^{-3} and σ_θ = 25.8 kg m^{-3} contours in Figure 9), indicating that the subsurface maximum is a result of predominantly isopycnal processes. North of ~40°N, along the northern edge of the subtropical gyre and within the subpolar gyre, the density of the CFC-12 maximum in the model (Figure 9a) mirrors the shape of the winter mixed layer density (Figure 2), with the maximum at each grid point occurring at the density of the shallowest existing model layer. This is consistent with the idea that the subsurface CFC maxima in this region are remnants of the winter mixed layer [*Warner et al.*, 1996; *Mecking and Warner*, 2001]. However, the density of the modeled CFC-12 maximum in the subpolar region is somewhat greater than observed (Figure 9b), partly because of the limited layer resolution in the model. In addition, the winter mixed layer densities during the observations may differ from the climatology.

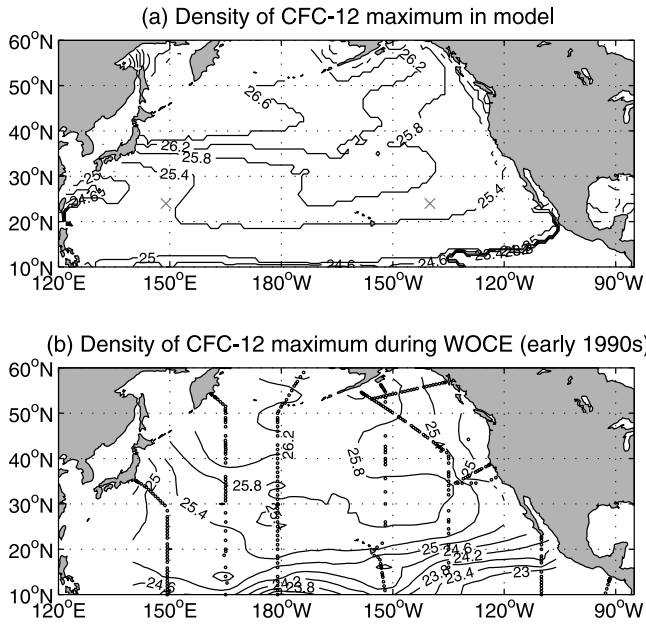

Figure 9. Potential density anomaly of subsurface CFC-12 concentration maximum (a) in the model in 1993 (diffusion case K2000/5000) and (b) during the early 1990s U.S. WOCE sections [adapted from *Mecking and Warner*, 2001]. Crosses in Figure 9a mark locations of the CFC-12 time series shown in Figure 10. Dots in Figure 9b indicate locations of data used.

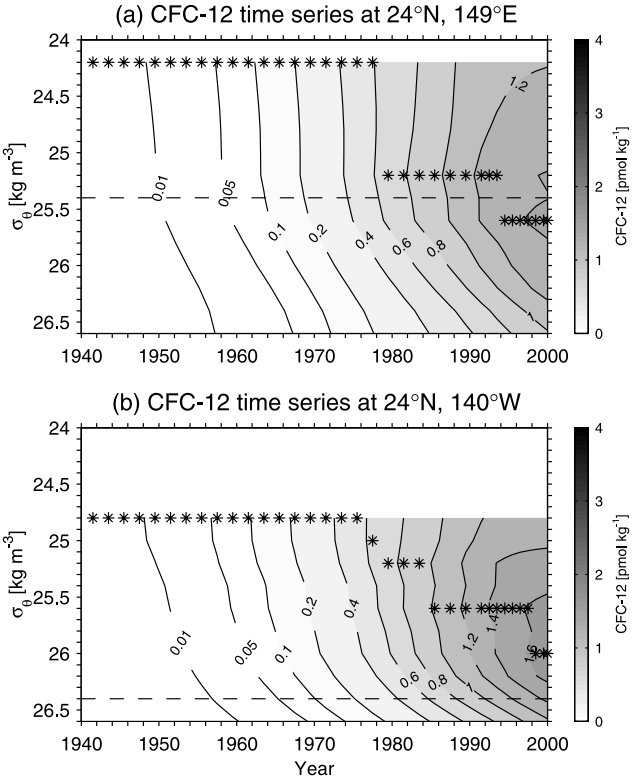

Figure 10. Time series of CFC-12 concentration from model (diffusion case K2000/5000) in (a) the western subtropical gyre (24°N, 149°E) and (b) the eastern subtropical gyre (24°N, 140°W). See Figure 9a for the location of the time series. Asterisks indicate the density of the main, vertical CFC-12 maximum (i.e., the density with the highest CFC-12 concentrations) at each point in time. Dashed lines mark the bottom of the advectively ventilated thermocline (see Figure 4) at the locations of the time series.

[28] In the subtropical gyre, where the CFC-12 maximum is a permanently subducted feature, model time series at two locations in the western and eastern subtropical North Pacific (at 149°E, 24°N, and 140°W, 24°N, respectively) show the density of the CFC-12 maximum increasing with time (Figure 10). Since the advection-diffusion model assumes a steady state circulation, this confirms that the deepening of the CFC-12 maximum versus density is due to the shape of the time-dependent atmospheric CFC time histories and not necessarily due to changes in oceanic processes [*Mecking and Warner*, 2001]. It also verifies that any collocations of the CFC maxima with North Pacific water masses, in particular with the mode waters, are only temporary. At the location in the western North Pacific, for instance, the early 1990s CFC-12 maximum is found in the model just above the bottom of the advectively ventilated thermocline at σ_θ = 25.2 kg m^{-3} (Figure 10a), which corresponds to the density of STMW at this location [*Mecking and Warner*, 2001]. By 2000, that maximum has moved below the advectively ventilated thermocline (and STMW), suggesting that it is now located within the corresponding isopycnal's diffusively ventilated WSZ. In the eastern North Pacific the CFC-12 maximum in 2000 remains above the bottom of the ventilated thermocline (Figure 10b), whose density is greater here than in the west. However, in the future, the maximum in the east is likely to move to greater densities as well through the diffusive ventilation process.

4.2. CFC-12 Inventories and Water Mass Formation Rates

[29] CFC inventories have been used to estimate water mass formation rates by relating the total inventory of a volume of water (I) to the water mass formation rate (R) through $I = \int \rho R C_{\text{input}} dt - L$ [cf. *Orsi et al.*, 1999], where the integration is from the time when CFCs were first introduced into the atmosphere (1930s) to time of the measurement. C_{input} is the concentration of the water entering the volume of water, usually from the mixed layer. L, which describes the loss of CFCs from the volume of water during the integration period, is often assumed to be small for deep and bottom water masses [*Orsi et al.*, 1999; *Smethie and Fine*, 2001]. In the North Pacific subtropical thermocline, however, the CFCs in the water leaving the domain through obduction in the Kuroshio/Kuroshio Extension region [*Huang and Qiu*, 1994; *Qiu and Huang*, 1995] and advection/diffusion across 10°N are not negligible, and the loss term needs to be estimated when calculating subduction rates in density classes (J. L. Bullister et al., manuscript in preparation, 2004). In addition, CFC input through diffusive ventilation is important in the North Pacific thermocline.

[30] To illustrate how CFC inventories are affected by isopycnal mixing, we compare vertical CFC-12 layer inventories, calculated as the CFC-12 concentration fields times isopycnal layer thickness (see section 2.3) and density, for model results with and without diffusion. In the advection-only case, a minimum in inventory occurs within the WSZ of σ_θ = 26.0 kg m^{-3} (Figure 11a) because this region remains largely unventilated in the absence of diffusion (Figure 6a). When isopycnal mixing is included, the inventory minimum within the WSZ is filled in (Figure 11b), and the vertical layer inventories in this case are in good agreement with the inventories based on the WOCE data (Figure 11c). The inventory maximum near the outcrop in the central Pacific in Figures 11b and 11c, not apparent in the corresponding concentrations fields (Figures 7c and 6d, respectively), corresponds to a maximum in layer thickness (not shown) and reflects the importance of spatial layer thickness variations in determining the inventory distributions.

[31] Integrating the vertical layer inventories for all modeled isopycnals over the area of the subtropical gyre (10°N to the wintertime outcrop or 45°N, whichever is farther south) shows that for isopycnals $\leq$25.4 kg m^{-3} the model's total layer inventories with and without diffusion agree well with the observations (Figure 12). For denser isopycnals that have substantial WSZs the advective-diffusive model and observed inventories are increasingly larger than the advection-only model inventories. The advective-diffusive inventories exceed those based on advection alone by 10% for σ_θ = 25.6 kg m^{-3}, 18% for σ_θ = 25.8 kg m^{-3}, 30% for σ_θ = 26.0 kg m^{-3}, and on the order of 50% for σ_θ = 26.2–26.6 kg m^{-3}. Since grid-size-induced mixing in the WBC carries some tracer into the WSZs (see section 3.1), advective inventories are also calculated for model cases using

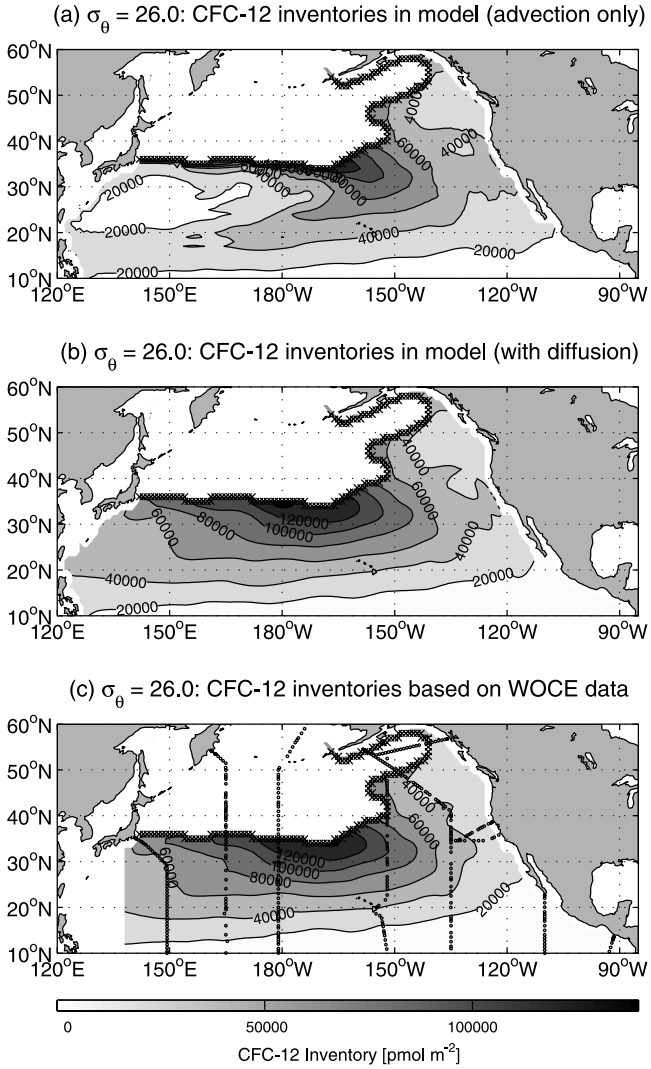

Figure 11. Vertical CFC-12 layer inventories for σ_θ = 26.0 kg m^{-3}: CFC-12 concentrations are (a) from model experiments using advection only (Figure 6a, except that 90% outcrop saturation is assumed), (b) from model experiments including advection and diffusion (diffusion case K2000/5000; Figure 7c), and (c) from the early 1990s U.S. WOCE sections corrected to 1993 (Figure 6d). Layer thickness is determined from the Levitus 1994 climatology (see text). Crosses mark March outcrop locations of isopycnal. Dots in Figure 11c indicate locations of WOCE data used. Data to the north/northwest of the isopycnal outcrop have been omitted.

advection fields without WBC, for which the westward flow in the NEC ends at the western boundary (not shown). In this case the additional inventory provided by the advective-diffusive model is even larger, ranging from 20% for σ_θ = 25.6 kg m^{-3} to 130% for σ_θ = 26.6 kg m^{-3}.

[32] The model suggests that ventilation through isopycnal mixing provides a significant contribution to the CFC-12 inventories for $\sigma_\theta \geq 25.6$ kg m^{-3}. Hence subduction rates calculated from observed CFC inventories for these isopycnals (assuming, for instance, that the loss term is also proportional to the subduction rate [*Sarmiento*, 1983]) will exceed those based on advective ventilation processes only, such as Ekman pumping and lateral induction at the outcrops [*Huang and Qiu*, 1994; *Qiu and Huang*, 1995]. In this regard, it is not surprising that water mass renewal times reported by *Huang and Qiu* [1994] for σ_θ = 26.0 kg m^{-3} and σ_θ = 26.4 kg m^{-3} are much larger than ventilation timescales based on pCFC-11 ages [*Warner et al.*, 1996]. The difference in timescales results from including the WSZ volumes in the subduction rate estimates based on Ekman pumping and lateral induction [*Huang and Qiu*, 1994], even though the water in the WSZs is not renewed through direct advection from the outcrops. Thus in the context of water mass renewal it is important to distinguish between directly ventilated regions and regions that are isolated from advective ventilation [*Huang and Russell*, 1994].

[33] The advective subduction rates are adequate when looking at net mass transport onto an isopycnal. In contrast, subduction rates or turnover times based on CFC inventories include diffusive processes and are more appropriate for describing fluxes of not only CFCs but also of other diffusively transported properties like oxygen, CO_2, and heat, though tracer gradients may vary. However, estimation of the CFC loss term is problematic, and CFC inventories can only constrain thermocline subduction rates to a range of values, each based on different assumptions for the loss term (J. L. Bullister et al., manuscript in preparation, 2004).

4.3. CFC Age Biases

[34] CFC ages can be inferred from the modeled tracer distributions using equation (1) and projecting the resulting pCFC-12, pCFC-11, or pCFC-11/pCFC-12 ratio onto the

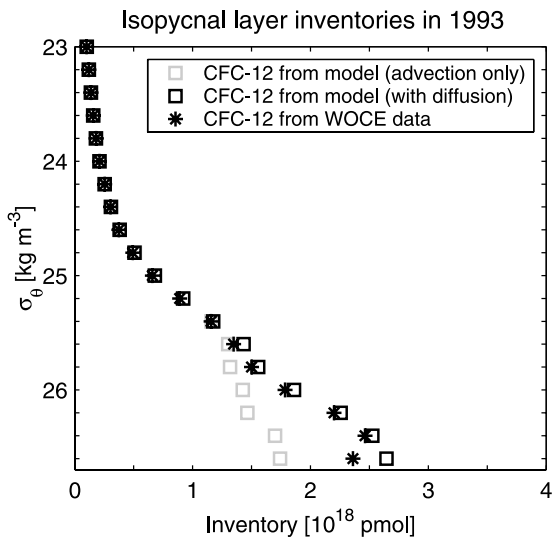

Figure 12. Isopycnal layer inventories of CFC-12 in 1993 for the subtropical gyre (south of 45°N/isopycnal outcrops): CFC-12 concentrations are from model experiments using advection only (shaded squares), from model experiments including advection and isopycnal diffusion (diffusion case K2000/5000, solid squares), and from the early 1990s U.S. WOCE data (corrected to 1993, asterisks). Layer thicknesses are determined from the Levitus 1994 climatology (see text).

atmospheric time histories (see section 1). This requires knowing the solubility at each grid point, which in turn requires propagating the solubility or temperature and salinity (from which solubility can be inferred) from the outcrops into the ocean interior. Since age biases due to solubility effects are of second order compared to biases due to the nonlinear atmospheric curves [*Doney et al.*, 1997; *Mecking*, 2001], a simpler approach is to use pCFC-12 and pCFC-11 rather than the CFC concentrations when integrating the advection-diffusion equation (4). The outcrop boundary condition, in this case, is prescribed by the atmospheric CFC partial pressures times the saturation factor ($X_{atmos} \cdot f_{sat}$). Because the choice of saturation factor has no significant effect on the resulting pCFC ages (as long as it is also accounted for when calculating the ages from the modeled tracer fields [*Mecking*, 2001]), air-sea equilibrium ($f_{sat} = 1$) is assumed for all isopycnals during the pCFC integrations. At the southern boundary (10°N) the pCFC values are set to the atmospheric CFC concentrations at an earlier time determined by the age boundary condition (see section 2.2).

[35] To evaluate biases in the CFC ages, we compare them with the "true" or ideal age, which is the advective age of the water modified only by linear age mixing with the surrounding waters. However, the ideal ages on $\sigma_\theta \geq 26.2$ kg m^{-3} are sensitive to the ages at 10°N (see section 2.2), so the age biases on these isopycnals depend on the southern boundary condition. With a simple, one-dimensional model, *Sonnerup* [2001] estimated that pCFC ages of ~30 years may underestimate ideal ages by 60–100% for the North Pacific WOCE cruise along 152°W (P16). On the basis of these ballpark estimates, experiments are done with the advection-diffusion model, in which the age boundary condition (Figure 5) is multiplied by factors 1.5 and 2. The integrations for ideal age as well as pCFC-12 and pCFC-11 are all performed using diffusion case K2000/5000.

4.3.1. pCFC-12 and pCFC-11 Ages

[36] The modeled ideal age and pCFC-12 age fields on $\sigma_\theta = 26.0$ kg m^{-3} are nearly identical in 1993 (Figures 13a and 13b) and are in good agreement with the observed pCFC-12 ages (Figure 13c), though the observed ages (determined using $f_{sat} = 0.9$, the best-fit saturation factor for $\sigma_\theta = 26.0$ kg m^{-3}, in equation (1)) remain greater than zero along parts of the outcrop. The relationship between pCFC-12 ages and ideal ages, however, evolves over time (Figure 14). In 1980 the pCFC-12 ages on $\sigma_\theta = 26.0$ kg m^{-3} are biased young by as much as 2 years in the western subtropical gyre (Figure 14a), where ventilation through mixing predominates in the WSZ. These biases are consistent with the positive (upward) curvature of the atmospheric time histories prior to 1980, which causes the pCFC-12 age corresponding to the mixture of two end-members to be less than the average age (Figure 1a). Ages of pCFC-12 in 1980 are also younger than ideal ages by more than 1 year along the southern boundary, particularly in the southeastern corner of the subtropical gyre. Although large age biases may be expected for mixing with older waters entering the model domain in the southeast (Figure 3), the values of the age biases in this region cannot be considered accurate due to the influence of the southern boundary extending to about

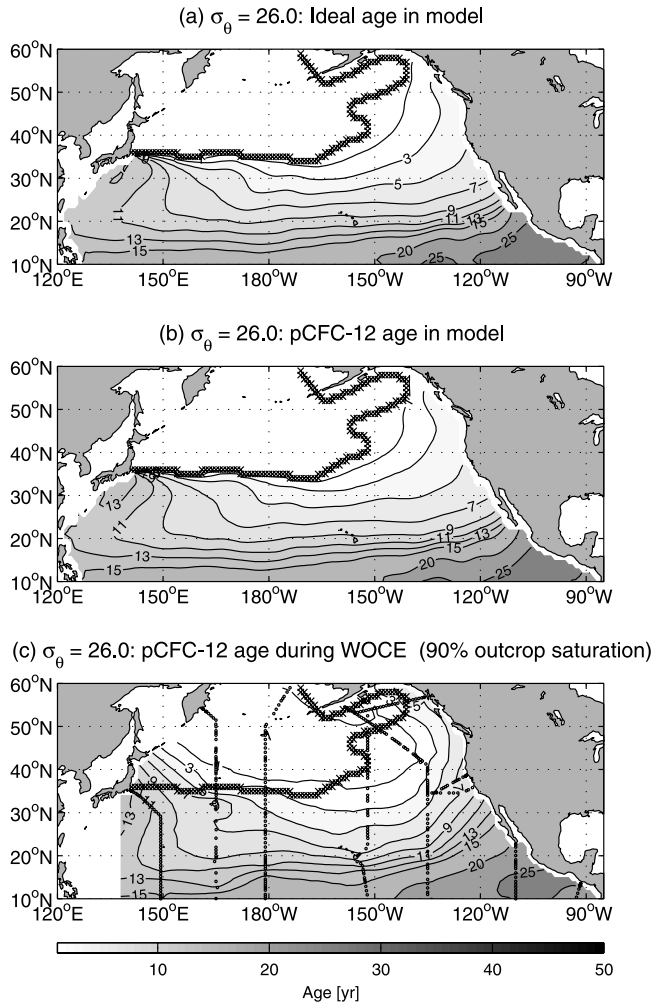

Figure 13. Age distributions on $\sigma_\theta = 26.0$ kg m^{-3}: (a) ideal age from model (diffusion case K2000/5000), (b) pCFC-12 age in 1993 based on pCFC-12 from model (diffusion case K2000/5000), and (c) pCFC-12 age during the early 1990s U.S. WOCE sections (assuming an outcrop saturation of 90% in equation (1) when converting CFC concentrations to pCFC). Crosses mark March outcrop locations of isopycnal. Dots in Figure 13c indicate locations of data used.

18°N on $\sigma_\theta = 26.0$ kg m^{-3} (see section 2.2). In 1987 (the midpoint of a pre-WOCE North Pacific survey [*Warner et al.*, 1996]) the age biases are reduced to <1 year, except in the southeast corner and in other parts of the southern boundary region (Figure 14b). This reflects the more constant increase in atmospheric CFC concentrations prior to this time (Figure 1a). The age differences in 1993 are also small (Figure 14c), as indicated by Figures 13a and 13b. However, pCFC-12 ages are greater than ideal ages now by more than 1 year in a small area near the isopycnal outcrop in the western subtropical gyre, reflecting the reversal in curvature of the CFC time histories from positive to negative in the late 1980s (Figure 1a). Because of this change in curvature and the associated decrease in atmospheric CFC growth rates, pCFC-12 ages are biased old over large portions of the subtropical gyre in 2000 (Figure 14d).

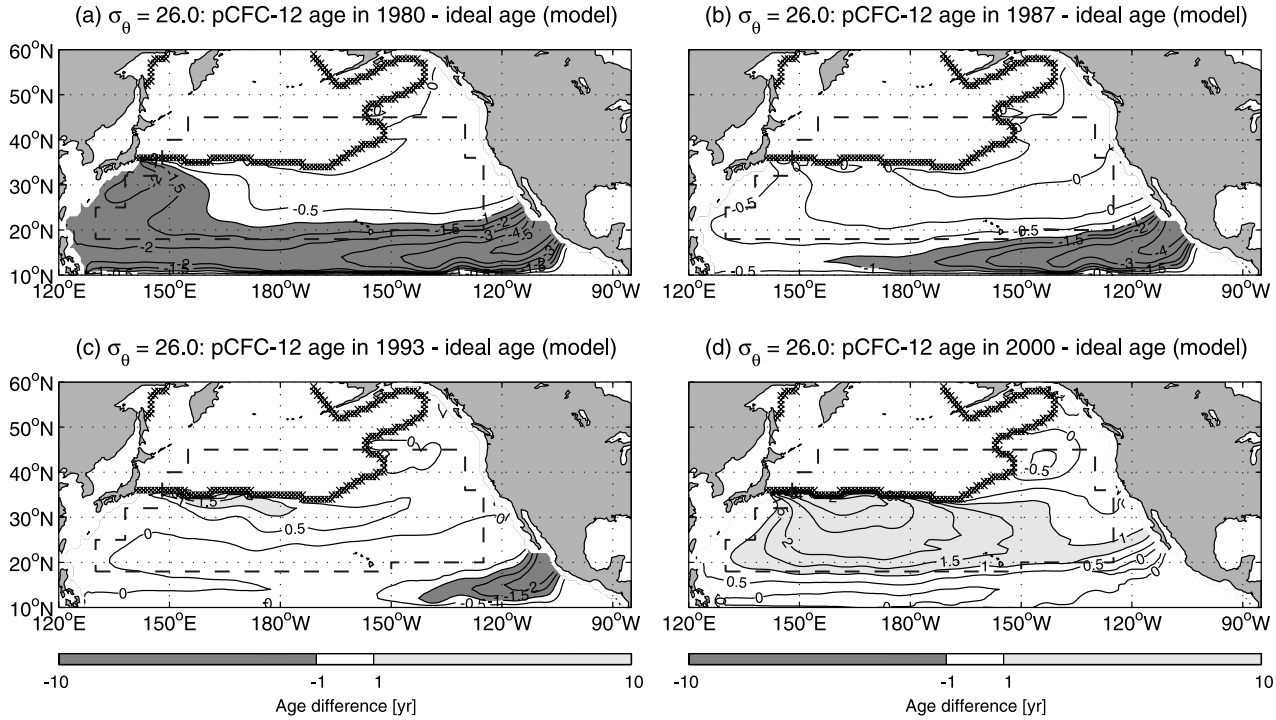

Figure 14. Difference between ideal age and pCFC-12 ages in model (diffusion case K2000/5000) on $\sigma_\theta = 26.0$ kg m^{-3}: (a) pCFC-12 age−ideal age in 1980, (b) pCFC-12 age−ideal age in 1987 (midpoint of pre-WOCE survey described by *Warner et al.* [1996]), (c) pCFC-12 age−ideal age in 1993 (midpoint of early 1990s WOCE period), and (d) pCFC-12 age−ideal age in 2000. Dark shading marks age differences less than −1 years, light shading marks age differences greater than 1 year, and age differences between −1 and 1 year have no shading. Crosses mark March outcrop locations of isopycnal. Dashed lines mark the area used for the CFC age−ideal age plots in Figures 15–17.

[37] The temporal evolution of the pCFC-12 ages in the model is summarized for all isopycnals in diagrams of pCFC-12 age versus ideal age (Figure 15). Since ideal ages on the denser isopycnals ($\sigma_\theta \geq 26.2$ kg m^{-3}) are affected by the southern boundary condition beyond 18°N (see section 2.2), the southern limit of the points included in the age diagrams (see dashed lines in Figure 14), results are plotted for three scenarios: ages set to 1.0, 1.5, and 2.0 times the WOCE pCFC-12 ages at 10°N. The evolution of the pCFC-12 ages is conceptually the same for all three model experiments and follows the discussion above: In 1980 the age biases are toward younger pCFC-12 ages for all ages (Figure 15a) because of the positive curvature of the atmospheric time histories. In 1987, there is less scatter in the pCFC-12 age−ideal age relationship (Figure 15b), and pCFC-12 ages become closer to ideal ages as the atmospheric time history becomes linear. Because of the reduction in atmospheric growth rates, biasing toward older pCFC-12 ages occurs in 1993 for ideal ages <5 years (Figure 15c). Older ages continue to move closer to ideal ages, with pCFC-12 ages of ~25 years now being biased young by 8/16/24 years for the age factors of 1.0/1.5/2, respectively, used at the southern boundary. This corresponds to a maximum underestimation of the ideal ages of 25%, 40%, and 50%, respectively, in 1993. The trend toward older pCFC-12 ages continues in 2000, when pCFC-12 ages <15 years are biased old by as much as 5 years and pCFC-12 ages >15 years are biased young by as much as much as 5–22 years for the age factors 1–2 (Figure 15d).

[38] The relationship between pCFC-11 ages and ideal ages (Figure 16) is very similar to the pCFC-12 age−ideal age relationship (Figure 15) until 1993. The positive curvature of the CFC-11 time history prior to the 1980s was somewhat greater (Figure 1a) so that pCFC-11 ages at the higher end of the age spectrum are biased young by as much as 1–2 years more than the pCFC-12 ages. Starting in the late 1980s, the atmospheric CFC-11 growth rates decreased faster than the CFC-12 growth rates so that biases toward older ages are slightly greater in 1993 for young pCFC-11 ages (Figure 16c) than for young pCFC-12 ages (Figure 15c). Because the atmospheric CFC-11 concentrations then began to decrease in the early 1990s, pCFC-11 ages less than ~10 years cannot be uniquely identified in 2000, and pCFC-11 ages just >10 years exceed ideal ages by as much as 10 years (i.e., they can correspond to ideal ages of close to zero years) (Figure 16d).

[39] Given that the early 1990s WOCE pCFC-12 ages used for the southern boundary condition for $\sigma_\theta \geq 26.2$ kg m^{-3}, ranging from 20 to 45 years (Figure 5), are evidently biased young (Figure 15c), the advection-diffusion model supports the assumption that increasing the ages at the boundary should provide more realistic ideal ages. For the multiplying factors of 1.5 and 2 the estimated age biases for pCFC-12 ages of 25 years amount to 16 years and 24 years, respectively, and are approximately self-

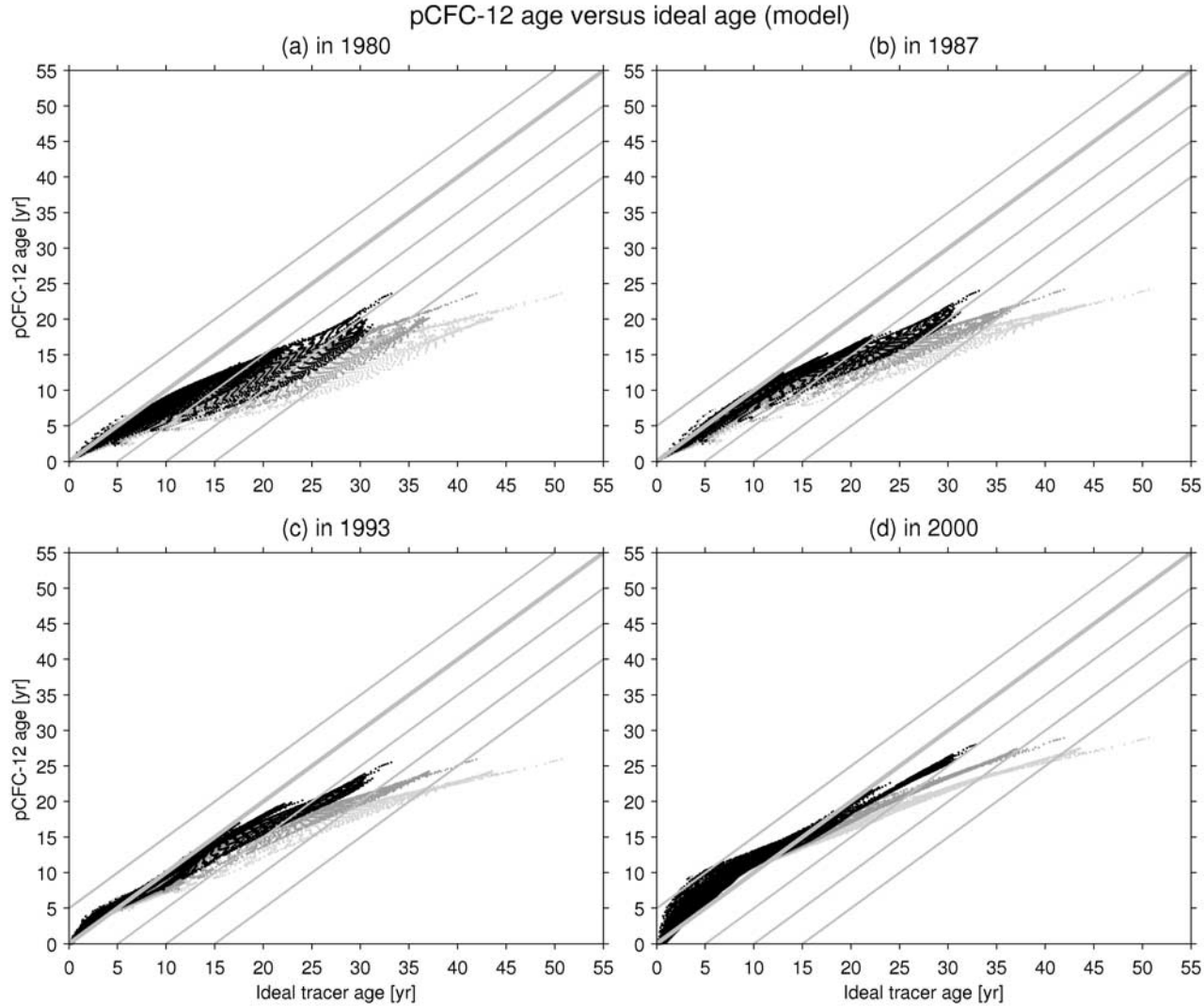

Figure 15. pCFC-12 age versus ideal age in model (diffusion case K2000/5000) for all modeled isopycnals (σ_0 = 23.0–26.6 kg m^{-3}) using pCFC-12 ages (a) in 1980, (b) in 1987, (c) in 1993, and (d) in 2000. Dark, intermediate, and light shading marks model runs where the age boundary condition at 10°N (based on WOCE pCFC-12 ages) has been multiplied by factors of 1, 1.5, and 2, respectively. Thick lines mark the equal age lines. Thin lines are drawn offset by 5 years. Only grid points within the subtropical region marked in Figure 14 are included.

consistent with the corrections applied at the boundary. Hence the pCFC age–ideal age relationships in Figures 15 and 16 based on these factors are expected to be the most realistic.

4.3.2. pCFC Ratio Ages

[40] The modeled pCFC-11 and pCFC-12 can be combined into the pCFC-11/pCFC-12 ratio to determine the age bias of the pCFC ratio age. The pCFC ratio ages have been used to define the age of the newly ventilated component, where deep and bottom waters are mixing into CFC-free older waters, such as along the deep western boundary in the North Atlantic [*Weiss et al.*, 1985]. In the North Pacific thermocline, where renewal timescales are <50 years (as indicated by the range of ideal ages in Figures 15–17), water that is newly subducted mixes with water that has borne CFCs for at least a couple decades. When waters with different pCFC ratios mix, two different biasing effects take place (see section 1). First, the ratio of the mixture is always biased toward the component with the higher CFC-12 concentrations (see Appendix A), which is also generally the younger component. On the other hand, the negative curvature of the atmospheric CFC-11/CFC-12 concentration history causes a bias toward older ages (Figure 1b).

[41] In the 1980 model results, pCFC ratio ages of 3–5 years are older than ideal ages, and biasing toward younger than ideal ages occurs for ratio ages >3–5 years (Figure 17a). In 1987 the transition between the two biasing effects occurs at a ratio age of 12–13 years, with the oldest ratio ages (~17 years) being younger than ideal ages by as much as 15–35 years (Figure 17b). Because the atmospheric CFC-11/CFC-12 concentration ratio leveled off in the 1970s and decreased in the 1990s (Figure 1b), unique determination of pCFC ratio ages is not possible for ratio ages less than ~3 years and ~12 years in 1980 and 1987 (Figure 17),

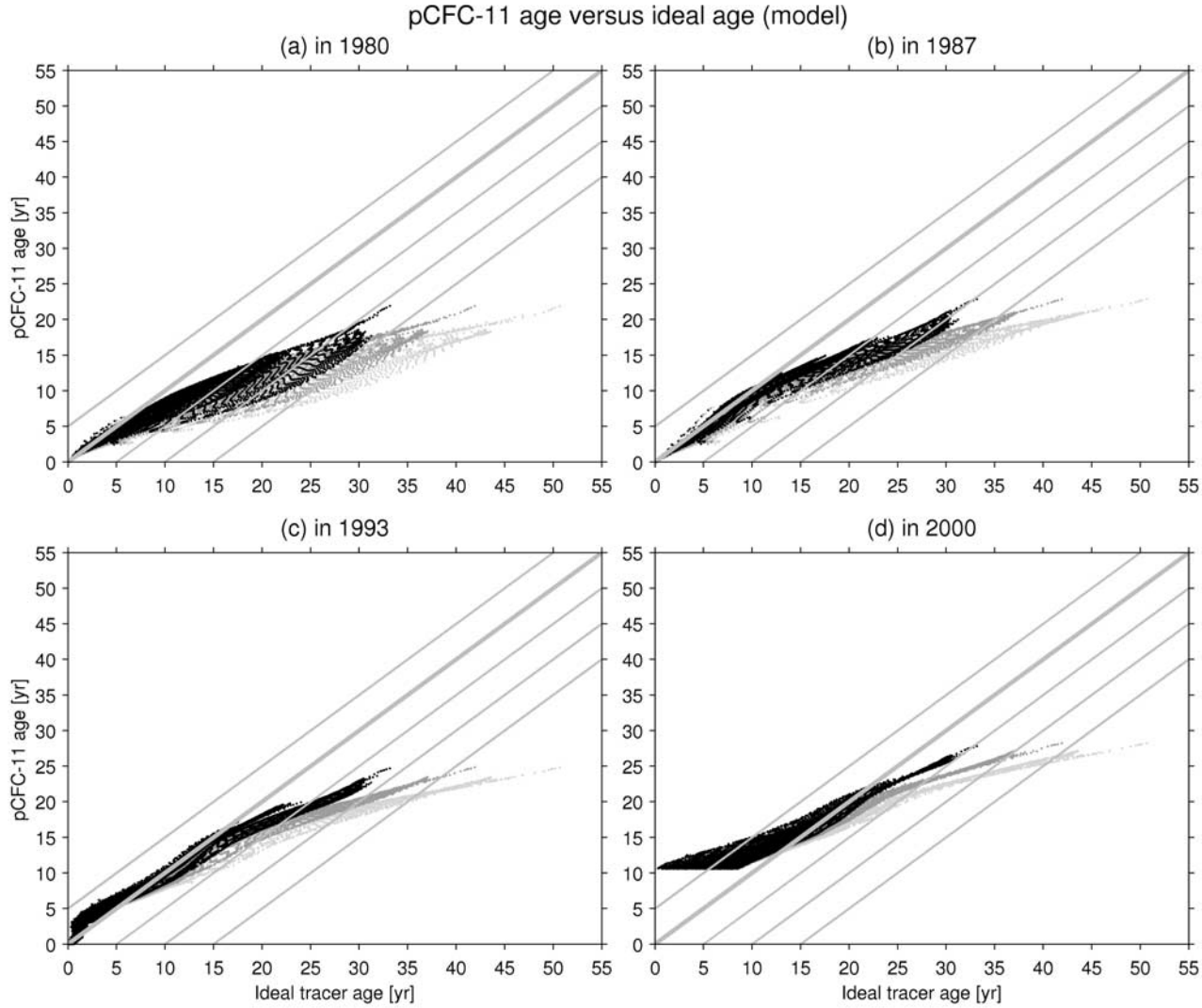

Figure 16. pCFC-11 age versus ideal age in model (diffusion case K2000/5000) for all modeled isopycnals (σ_θ = 23.0–26.6 kg m^{-3}) using pCFC-11 ages (a) in 1980, (b) in 1987, (c) in 1993, and (d) in 2000. Details follow Figure 15.

respectively, and for most of the model output in 1993 and 2000 (not shown). Hence pCFC ratio ages are only of limited use in the thermocline.

5. Discussion and Summary

[42] We used a diagnostic, isopycnal advection-diffusion model based on climatological, geostrophic velocity fields to investigate the effects of mixing on the distributions of CFCs for isopycnals that outcrop in the open North Pacific ($\sigma_\theta \leq$ 26.6 kg m^{-3}). The model is tuned by adjusting its isopycnal diffusion rate and the CFC saturation at the outcrops. The good agreement between the modeled CFC-12 fields and the early 1990s North Pacific U.S. WOCE CFC data (mapped onto isopycnal surfaces) in the subtropics confirms that purely isopycnal processes can explain tracer distributions in subtropical thermoclines. It also indicates that the CFC data and the climatological flow fields are consistent with each other, even though the Levitus climatology is highly smoothed and presumably not representative of the flow at any given time. This reflects the fact that the tracer data do not represent a snapshot of the flow either but the time-integrated flow instead. In the subpolar gyre the model simulates tracer distributions somewhat less well, likely because of the greater importance of the barotropic velocity component here and because salinity (poorly resolved in the climatological data) plays an important role in mixed layer depth and isopycnal structure there. Nevertheless, it is evident from both data and model maps of CFC-12 and from isopycnal streamlines that tracer is carried from the outcrops into the subpolar gyre as in the subtropics (Figures 3 and 6–8). This is contrary to the idea that the subpolar gyre is a region of Ekman suction and obduction, where water reenters the mixed layer from the thermocline [*Qiu and Huang*, 1995], and we suggest that the ventilation of the subpolar gyre may be subject of future investigations.

[43] Isopycnal diffusivities of 5000 m^2 s^{-1}, where the Kuroshio splits off Japan, and of 2000 m^2 s^{-1} elsewhere, together with outcrop saturations <100% for $\sigma_\theta >$ 25.2 kg m^{-3} (95% for σ_θ = 25.4–25.8 kg m^{-3}, 90% for

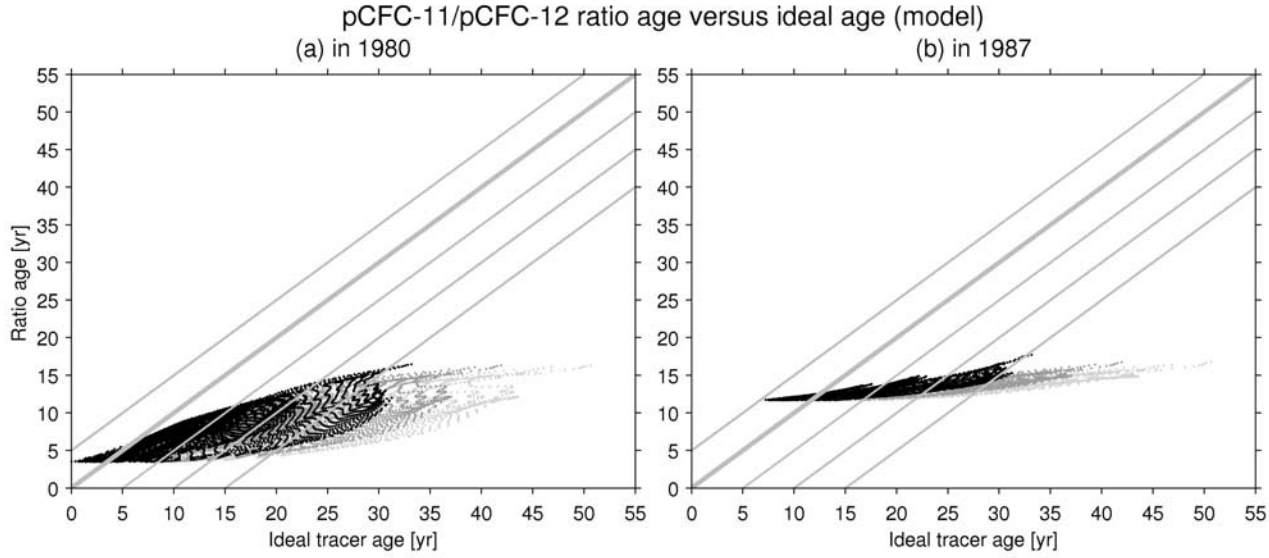

Figure 17. pCFC-11/pCFC-12 ratio age versus ideal age in model (diffusion case K2000/5000) for all modeled isopycnals (σ_θ = 23.0–26.6 kg m^{-3}) using ratio ages (a) in 1980 and (b) in 1987. Details follow Figure 15.

σ_θ = 26.0–26.2 kg m^{-3}, 85% for σ_θ = 26.4 kg m^{-3}, and 80% for σ_θ = 26.6 kg m^{-3}), give the best agreement between the early 1990s CFC data and the model. Enhanced diffusion in the Kuroshio Extension region and CFC undersaturations in the northwestern North Pacific, where winter mixed layers are deep, are reasonable assumptions. However, errors in the outcrop positions due to the bulk formula estimates of the isopycnal outcrops and interannual variations could have similar effects. In the model, isopycnal diffusion increases CFC inventories significantly on isopycnals with WSZs (also referred to as "pool regions" [*Luyten et al.*, 1983]) with the additional supply of CFC-12 inventory in the subtropics through diffusion ranging from 10–20% for σ_θ = 25.6 kg m^{-3} to 50–130% for σ_θ = 26.6 kg m^{-3} in 1993 relative to advection only. Thus the net transport of CFCs into the thermocline through isopycnal diffusion is important [*Sarmiento*, 1983; *Musgrave*, 1990] and must be considered when comparing subduction rates calculated from Ekman pumping and lateral induction [*Huang and Qiu*, 1994; *Qiu and Huang*, 1995] to those based on tracer budgets. Coupling of the isopycnal layers shows that vertical diffusion has little effect on the CFC distributions and cannot account for the ventilation of the WSZs. The model results also support the idea that the North Pacific CFC maxima are transient features that have been deepening and moving, through the isopycnal diffusion process, into the WSZs and below the density of STMW [*Mecking and Warner*, 2001]. They should therefore not be used as long-term indicators of mode waters.

[44] In the model results, age biases due to isopycnal mixing affect pCFC ratio ages more than pCFC-11 ages, which are affected slightly more than pCFC-12 ages. The results suggest that at the time of the North Pacific WOCE cruise (~1993), pCFC-12 ages <5 years were older than ideal ages by 0–2.5 years, whereas pCFC-12 ages >5 years were biased increasingly young. For the older ages, specification of the CFC age biases is complicated by the fact that the ideal ages on the denser isopycnals ($\sigma_\theta \geq$ 26.2 kg m^{-3}) are influenced by the age boundary condition at 10°N. Assuming that the observation-based pCFC-12 ages at 10°N, which are used to specify the boundary condition, are biased young themselves by 50–100% [*Sonnerup*, 2001], age biases for pCFC-12 ages of ~25 years in 1993 range from 16 to 24 years, implying that ideal ages are underestimated by as much as 40–50%. These model-derived age bias estimates, presented as difference maps between the CFC ages and the ideal ages (see Figure 14) and as diagrams of CFC ages versus ideal age (see Figures 15–17), can be used as corrections to observed CFC ages to estimate ages closer to ideal ages. While the age-age diagrams involve much scatter and hence uncertainties in the ideal ages of several years, they are a useful way of inferring ideal ages because they can be applied without assuming that the circulation patterns in the ocean are exactly the same as in the model.

[45] Accounting for the time-evolving age biases is necessary when investigating changes in observed CFC ages along repeated hydrographic sections [*Watanabe et al.*, 2001; Mecking et al., submitted manuscript, 2004]. In particular, an increase in observed pCFC-12 or pCFC-11 ages does not necessarily indicate a slowdown in oceanic ventilation because both pCFC-12 ages and pCFC-11 ages are becoming increasingly older due to the mixing bias effects. Only a CFC age change that is significantly different from the predicted difference in mixing biases between two sections can be interpreted as a true change in oceanic processes. When combining CFC ages with other measurements to infer biogeochemical rates and other quantities, nonlinear mixing effects in the other tracers and also in the derived property must be considered as well. For instance, while we suggest that it is better to use CFC ages corrected for mixing biases rather than uncorrected ages when estimating oxygen utilization rates (OURs) (as done by *Feely et al.* [2004]), it should be recognized that OUR is a ratio

(apparent oxygen utilization over age) that may mix nonlinearly (see Appendix A). For another common application of CFC ages, the determination of anthropogenic carbon inventories, for which pCFC ages are used to infer the inorganic carbon concentrations at the time when the water left the surface [*Gruber et al.*, 1996; *Sabine et al.*, 1999, 2002; *McNeil et al.*, 2003], a problem arises because carbon distributions in the ocean are also affected by nonlinear mixing themselves. Hence a conservative age tracer whose input function exactly resembles the one of CO_2 would be best to infer the oceanic uptake of anthropogenic carbon. In the absence of such a tracer, age spectra derived from a combination of age tracers may provide improved anthropogenic carbon estimates [*Hall et al.*, 2002]. On the other hand, it was found, on the basis of simulations with ocean general circulation models, that pCFC-11 or pCFC-12 ages give good predictions when determining recent decadal-scale changes in anthropogenic carbon inventories (rather than the total anthropogenic carbon content) for waters younger than 30 years [*Matear et al.*, 2003; *McNeil et al.*, 2003]. The ages of pCFC do well in this case because of the similarities in the shape of the atmospheric CFC and CO_2 time histories between 1970 and 1990.

Appendix A: Mixing of Ratios

[46] Consider two properties (A and B) and their ratios for two end-members ($R_1 = (A_1/B_1)$ and $R_2 = (A_2/B_2)$). The average ratio of the two end-members is then given by

$$R_{\text{ave}} = \frac{1}{2}\left(\frac{A_1}{B_1} + \frac{A_2}{B_2}\right). \tag{A1}$$

However, when the properties of the two end-members are mixed together, the ratio of the mixture, assuming that both properties mix linearly, is

$$R_{\text{mix}} = \frac{A_1 + A_2}{B_1 + B_2}, \tag{A2}$$

which is different from the average ratio equation (A1). This is because the mixing of ratios is nonlinear. To determine how the ratio of the mixture is biased due to this nonlinearity, R_{mix} is compared to R_{ave}. The goal is to determine whether the question mark in

$$R_{\text{mix}} \;?\; R_{\text{ave}} \tag{A3}$$

can be uniquely replaced by a $<$ or $>$ sign. Substituting equations (A1) and (A2) into equation (A3) gives

$$\frac{A_1 + A_2}{B_1 + B_2} \quad ? \quad \frac{1}{2}\left(\frac{A_1}{B_1} + \frac{A_2}{B_2}\right), \tag{A4}$$

which can be transformed to

$$0 \quad ? \quad (B_1A_2 - B_2A_1)(B_1 - B_2), \tag{A5}$$

assuming that B_1 and B_2 are both positive (otherwise the sign may change during the transformation). Defining end-member 1 to be the one with the greater value for property B (i.e., $B_1 > B_2$) allows to divide by $(B_1 - B_2)$ without any change in sign (i.e., the "?" still denotes the same sign as in equations (A3), (A4), and (A5)), which leads to

$$0 \quad ? \quad B_1A_2 - B_2A_1 \Leftrightarrow \frac{A_1}{B_1} ? \frac{A_2}{B_2}. \tag{A6}$$

If $R_1 > R_2$, it follows from equation (A6) in combination with equation (A3) that $R_{\text{mix}} > R_{\text{ave}}$. On the other hand, if $R_1 < R_2$, it follows that $R_{\text{mix}} < R_{\text{ave}}$. Hence R_{mix} is always biased toward the ratio of the end-member with the greater value for property B (in this case, end-member 1). This implies that the CFC-11/CFC-12 ratio is always biased toward the end-member with the greater CFC-12 concentrations, which usually (until the 1990s when the atmospheric CFC-11 concentrations began decreasing) also corresponds to the end-member with the greater CFC-11 concentrations. In the special case where $R_1 = R_2$ the bias is zero because $R_{\text{mix}} = R_{\text{ave}}$. Also, if $B_1 = B_2$, no biasing occurs because the two sides of equation (A4) are equivalent.

[47] **Acknowledgments.** We would like to thank LuAnne Thompson for much advice regarding the model development. Most of this work was performed while S.M. was a graduate student at the University of Washington under the support of NSF grant OCE-9819192. A postdoctoral scholarship for S.M. at the Woods Hole Oceanographic Institution, with funding provided by the Doherty Foundation, helped complete this work. R.E.S. acknowledges support from NSF grant OCE-0136897. This is WHOI contribution number 10958 and JISAO contribution number 1041.

References

Abell, J., S. Emerson, and P. Renaud (2000), Distributions of TOP, TON and TOC in the North Pacific subtropical gyre: Implications for nutrient supply in the surface ocean and remineralization in the upper thermocline, *J. Mar. Res.*, *58*, 203–222.

Armi, L., and H. M. Stommel (1983), Four views of a portion of the North Atlantic subtropical gyre, *J. Phys. Oceanogr.*, *13*, 828–857.

Bingham, F. M. (1992), Formation and spreading of Subtropical Mode Water in the North Pacific, *J. Geophys. Res.*, *97*, 11,177–11,189.

Cushman-Roisin, B. (1987), Subduction, in *Dynamics of the Oceanic Surface Mixed Layer*, special publication, edited by P. Müller and D. Henderson, pp. 181–196, Hawaii Inst. of Geophys., Honolulu.

Doney, S. C., and J. L. Bullister (1992), A chlorofluorocarbon section in the eastern North Atlantic, *Deep Sea Res., Part A*, *39*, 1857–1883.

Doney, S. C., W. J. Jenkins, and J. L. Bullister (1997), A comparison of tracer dating techniques on a meridional section in the eastern North Atlantic, *Deep Sea Res., Part I*, *44*, 603–626.

Doney, S. C., J. L. Bullister, and R. Wanninkhof (1998), Climatic variability in upper ocean ventilation rates diagnosed using chlorofluorocarbons, *Geophys. Res. Lett.*, *25*, 1399–1402.

Dutay, J.-C., et al. (2002), Evaluation of ocean model ventilation with CFC-11: Comparison of 13 global ocean models, *Ocean Modell.*, *4*, 89–120.

Emerson, S., Y. W. Watanabe, T. Ono, and S. Mecking (2004), Temporal trends in apparent oxygen utilization in the upper pycnocline of the North Pacific: 1980–2000, *J. Oceanogr.*, *60*, 139–147.

Feely, R. A., C. L. Sabine, R. Schlitzer, J. L. Bullister, S. Mecking, and D. Greeley (2004), Oxygen utilization and organic carbon remineralization in the Pacific Ocean, *J. Oceanogr.*, *60*, 45–52.

Fine, R. A. (1993), Circulation of Antarctic Intermediate Water in the south Indian Ocean, *Deep Sea Res., Part I*, *40*, 2021–2042.

Fine, R. A., R. Lukas, F. Bingham, M. J. Warner, and R. H. Gammon (1994), The western equatorial Pacific: A water mass crossroads, *J. Geophys. Res.*, *99*, 25,065–25,080.

Greene, C. E. (2000), The distribution of temperature and oxygen in a simple isopycnal model of subduction in the subtropical North Pacific: Implications for mixing and consumption, M.S. thesis, Univ. of Wash., Seattle.

Grey, S. M., K. Haines, and A. M. MacDonald (1999), Climatological hydrography of the North Atlantic, *Int. WOCE Newsl.*, *36*, 23–25.

Gruber, N., J. L. Sarmiento, and T. F. Stocker (1996), An improved method for detecting anthropogenic CO_2 in the oceans, *Global Biogeochem. Cycles*, *10*, 809–837.

Haine, T. W. N., and K. J. Richards (1995), The influence of the seasonal mixed layer on oceanic uptake of CFCs, *J. Geophys. Res.*, *100*, 10,727–10,744.

Hall, T. M., T. W. N. Haine, and D. W. Waugh (2002), Inferring the concentration of anthropogenic carbon in the ocean from tracers, *Global Biogeochem. Cycles*, *16*(4), 1131, doi:10.1029/2001GB001835.

Huang, R. X., and B. Qiu (1994), Three-dimensional structure of the wind-driven circulation in the subtropical North Pacific, *J. Phys. Oceanogr.*, *24*, 1608–1622.

Huang, R. X., and S. Russell (1994), Ventilation of the subtropical North Pacific, *J. Phys. Oceanogr.*, *24*, 2589–2605.

Iselin, C. O. (1939), The influence of vertical and lateral turbulence on the characteristics at mid-depths, *Eos Trans. AGU*, *20*, 414–417.

Jenkins, W. J. (1980), Tritium and ^{3}He in the Sargasso Sea, *J. Mar. Res.*, *38*, 533–569.

Jenkins, W. J. (1991), Determination of isopycnal diffusivity in the Sargasso Sea, *J. Phys. Oceanogr.*, *21*, 1058–1061.

Ledwell, J. R., A. J. Watson, and C. S. Law (1993), Evidence for slow mixing across the pycnocline from an open-ocean tracer release experiment, *Nature*, *364*, 701–703.

Ledwell, J. R., A. J. Watson, and C. S. Law (1998), Mixing of a tracer in the pycnocline, *J. Geophys. Res.*, *103*, 21,499–21,529.

Levitus, S. (1982), Climatological atlas of the world ocean, *NOAA Prof. Pap. 13*, 173 pp., U.S. Govt. Print. Office, Washington, D. C.

Levitus, S., and T. P. Boyer (1994), *World Ocean Atlas 1994*, vol. 4, *Temperature, NOAA Atlas NESDIS 4*, 129 pp., Natl. Oceanogr. Data Cent., Silver Spring, Md.

Levitus, S., R. Burgett, and T. P. Boyer (1994), *World Ocean Atlas 1994*, vol. 3, *Salinity, NOAA Atlas NESDIS 3*, 111 pp., Natl. Oceanic and Atmos. Admin., Silver Spring, Md.

Luyten, J. R., J. Pedlosky, and H. Stommel (1983), The ventilated thermocline, *J. Phys. Oceanogr.*, *13*, 292–309.

MacDonald, A. M., T. Suga, and R. G. Curry (2001), An isopycnally averaged North Pacific climatology, *J. Atmos. Oceanic Technol.*, *18*, 394–420.

Matear, R. J., C. S. Wong, and L. Xie (2003), Can CFCs be used to determine anthropogenic CO_2?, *Global Biogeochem. Cycles*, *17*(1), 1013, doi:10.1029/2001GB001415.

McNeil, B. I., R. J. Matear, R. M. Key, J. L. Bullister, and J. L. Sarmiento (2003), Anthropogenic CO_2 uptake by the ocean based on the global chlorofluorocarbon data set, *Science*, *299*, 235–239.

Mecking, S. (2001), Spatial and temporal patterns of chlorofluorocarbons in the North Pacific thermocline: A data and modeling study, Ph.D. thesis, 272 pp., Univ. of Wash., Seattle.

Mecking, S., and M. J. Warner (2001), On the subsurface CFC maxima in the subtropical North Pacific thermocline and their relation to mode waters and oxygen maxima, *J. Geophys. Res.*, *106*, 22,179–22,198.

Min, D.-H., J. L. Bullister, and R. F. Weiss (2000), Constant ventilation age of thermocline water in the eastern subtropical North Pacific Ocean from chlorofluorocarbon measurements over a 12-year period, *Geophys. Res. Lett.*, *27*, 3909–3912.

Montgomery, R. B. (1937), A suggested method for representing gradient flow in isentropic surfaces, *Bull. Am. Meteorol. Soc.*, *18*, 210–212.

Musgrave, D. L. (1985), A numerical study of the role of subgyre-scale mixing and the western boundary current on homogenization of a passive tracer, *J. Geophys. Res.*, *90*, 7037–7043.

Musgrave, D. L. (1990), Numerical studies of tritium and helium-3 in the thermocline, *J. Phys. Oceanogr.*, *20*, 344–373.

Orsi, A. H., G. C. Johnson, and J. L. Bullister (1999), Circulation, mixing, and production of Antarctic Bottom Water, *Prog. Oceanogr.*, *43*, 55–109.

Qiu, B. (1995), Why is the spreading of North Pacific Intermediate Water confined on density surfaces around $\sigma_\theta = 26.8$?, *J. Phys. Oceanogr.*, *25*, 168–180.

Qiu, B., and R. X. Huang (1995), Ventilation of the North Atlantic and the North Pacific: Subduction versus obduction, *J. Phys. Oceanogr.*, *25*, 2374–2390.

Qu, T., H. Mitsudera, and T. Yamagata (1998), On the western boundary currents in the Philippine Sea, *J. Geophys. Res.*, *103*, 7537–7548.

Reid, J. L. (1961), On the geostrophic flow at the surface of the Pacific Ocean with respect to the 1000-decibar surface, *Tellus*, *13*, 488–502.

Reid, J. L. (1965), Intermediate waters of the Pacific Ocean, *Johns Hopkins Oceanogr. Stud.*, *2*, 85 pp.

Reid, J. L. (1997), On the total geostrophic circulation of the Pacific Ocean: Flow patterns, tracers, and transports, *Prog. Oceanogr.*, *39*, 263–352.

Robbins, P. E. (1997), Temporal evolution of tritium-^{3}He age in the North Atlantic: Implications for thermocline ventilation, Ph.D. thesis, Woods Hole Oceanogr. Inst., Woods Hole, Mass.

Robbins, P. E., J. F. Price, W. B. Owens, and W. J. Jenkins (2000), The importance of lateral diffusion for the ventilation of the lower thermocline in the subtropical North Atlantic, *J. Phys. Oceanogr.*, *30*, 67–89.

Sabine, C. L., R. M. Key, K. M. Johnson, F. J. Millero, A. Poisson, J. L. Sarmiento, D. W. R. Wallace, and C. D. Winn (1999), Anthropogenic CO_2 inventory of the Indian Ocean, *Global Biogeochem. Cycles*, *13*, 179–198.

Sabine, C. L., R. A. Feely, R. M. Key, J. L. Bullister, F. J. Millero, K. Lee, T.-H. Peng, B. Tilbrook, T. Ono, and C. S. Wong (2002), Distribution of anthropogenic CO_2 in the Pacific Ocean, *Global Biogeochem. Cycles*, *16*(4), 1083, doi:10.1029/2001GB001639.

Sarmiento, J. L. (1983), A tritium box model of the North Atlantic thermocline, *J. Phys. Oceanogr.*, *13*, 1269–1274.

Smethie, W. M., Jr., and R. A. Fine (2001), Rates of North Atlantic Deep Water formation calculated from chlorofluorocarbon inventories, *Deep Sea Res., Part I*, *48*, 189–215.

Smethie, W. M., Jr., R. A. Fine, A. Putzka, and E. P. Jones (2000), Tracing the flow of North Atlantic Deep Water using chlorofluorocarbons, *J. Geophys. Res.*, *105*, 14,297–14,323.

Smolarkiewicz, P. K. (1984), A fully multi-dimensional positive definite advection transport algorithm with small implicit diffusion, *J. Comput. Phys.*, *54*, 325–362.

Sonnerup, R. E. (2001), On the relations among CFC derived water mass ages, *Geophys. Res. Lett.*, *28*, 1739–1742.

Sonnerup, R. E., P. D. Quay, and J. L. Bullister (1999), Thermocline ventilation and oxygen utilization rates in the subtropical North Pacific based on CFC distributions during WOCE, *Deep Sea Res., Part I*, *46*, 777–805.

Stammer, D. (1997), Global characteristic of ocean variability estimated from regional TOPEX/POSEIDON altimeter measurements, *J. Phys. Oceanogr.*, *27*, 1743–1769.

Stommel, H. (1979), Determination of water mass properties pumped down from the Ekman layer to the geostrophic flow below, *Proc. Natl. Acad. Sci. U. S. A.*, *76*, 537–558.

Thiele, G., and J. L. Sarmiento (1990), Tracer dating and ocean ventilation, *J. Geophys. Res.*, *95*, 9377–9391.

Walker, S. J., R. F. Weiss, and P. K. Salameh (2000), Reconstructed histories of the annual mean atmospheric mole fractions for the halocarbons CFC-11, CFC-12, CFC-113, and carbon tetrachloride, *J. Geophys. Res.*, *105*, 14,285–14,296.

Warner, M. J., and R. F. Weiss (1985), Solubilities of chlorofluorocarbons 11 and 12 in water and sea water, *Deep Sea Res., Part A*, *32*, 1485–1497.

Warner, M. J., and R. F. Weiss (1992), Chlorofluoromethanes in South Atlantic Antarctic Intermediate Water, *Deep Sea Res., Part A*, *39*, 2053–2075.

Warner, M. J., J. L. Bullister, D. P. Wisegarver, R. H. Gammon, and R. F. Weiss (1996), Basin-wide distributions of chlorofluorocarbons CFC-11 and CFC-12 in the North Pacific: 1985–1989, *J. Geophys. Res.*, *101*, 20,525–20,542.

Watanabe, Y. W., T. Ono, and A. Shimamoto (2000), Increase in the uptake rate of oceanic anthropogenic carbon in the North Pacific determined by CFC ages, *Mar. Chem.*, *72*, 297–315.

Watanabe, Y. W., T. Ono, A. Shimamoto, T. Sugimoto, M. Wakita, and S. Watanabe (2001), Probability of a reduction in the formation rate of the subsurface water in the North Pacific during the 1980s and 1990s, *Geophys. Res. Lett.*, *28*, 3289–3292.

Weiss, R., J. L. Bullister, R. H. Gammon, and M. J. Warner (1985), Atmospheric chlorofluoromethanes in the deep equatorial Atlantic, *Nature*, *314*, 608–610.

World Ocean Circulation Experiment Data Products Committee (WOCEDPC) (2002), WOCE global data, vers. 3.0, *Rep. 180/02*, World Ocean Circ. Exper. Int. Prod. Off., Southampton, U. K.

Wyrtki, K., L. Magaard, and J. Hager (1976), Eddy energy in the ocean, *J. Geophys. Res.*, *81*, 2641–2646.

Yuan, X., and L. D. Talley (1992), Shallow salinity minima in the North Pacific, *J. Phys. Oceanogr.*, *22*, 1302–1315.

C. E. Greene, S. L. Hautala, and M. J. Warner, School of Oceanography, University of Washington, Box 355351, Seattle, WA 98195-5351, USA. (greene@nasw.org; susanh@ocean.washington.edu; mwarner@ocean.washington.edu)

S. Mecking, Woods Hole Oceanographic Institution, 360 Woods Hole Road, Woods Hole, MA 02543, USA. (smecking@whoi.edu)

R. E. Sonnerup, Joint Institute for the Study of the Atmosphere and Ocean, University of Washington, Box 354235, Seattle, WA 98195-4235, USA. (rolf.sonnerup@noaa.gov)